九州大学学術情報リポジトリ
Kyushu University Institutional Repository

SHIP MOTIONS IN RESTRICTED WATERS: Tank Tests

Tasai, Fukuzo
Research Institute for Applied Mechanics, Kyushu Universily : Professor

Takaki, Mikio
Research Institute for Applied Mechanics, Kyushu University : Research Associate

Ohkusu, Makoto
Research Institute for Applied Mechanics, Kyushu University : Associate Professor

https://doi.org/10.5109/6617893

出版情報：Reports of Research Institute for Applied Mechanics. 26 (81), pp.23-81, 1978-07. 九州大学応用力学研究所
バージョン：
権利関係：

KYUSHU UNIVERSITY

Reports of Research Institute for Applied Mechanics
Vol. XXVI, No. 81, 1978

SHIP MOTIONS IN RESTRICTED WATERS
—Tank Tests—

By Fukuzo TASAI*, Mikio TAKAKI** and Makoto OHKUSU***

We measured radiation forces and wave exciting forces acting on a ship model in a canal and measured amplitudes of ship motions in regular waves. Those experimental results are compared with theoretical ones obtained by so-called "New Strip Method". The reasons for the difference of response curves of ship motions in regular waves between restricted waters and open sea are mostly made clear by experiments and theoretical considerations done in this investigation.

1. Introduction

It has been well known since early time that motions of a ship model and hydrodynamic forces acting on her are affected by interference of tank wall due to reflection from tank wall of waves generated by her motions in an experimental long tank. It is an important problem to predict these interferences of tank walls quantitatively in order to know characteristics of ship motions in open sea from an experimental study at a long water tank. It is also necessary to take effect of water depth into account in addition to effect of water breadth, if a long tank is a shallow depth. The condition of restricted breadth and restricted water depth is equivalent to that for an actual ship operating in a canal or a channel.

Hanaoka[1] and Hosoda[2] studied theoretically interference of tank wall affecting longitudinal motions of a ship in water of infinite depth, while Vossers & Swaan,[3] Murdy[4] and Takezawa & Jingu[5] investigated experimentally on it. Hanaoka evaluated hydrodynamic forces acting on a ship model and predicted longitudinal motions of a thin ship in regular waves by a method, in which three-dimensional effect on motions of a ship with a forward speed is taken into account and the boundary condition on tank walls is satisfied by taking virtual images of the ship model with respect to tank walls[1]. Takezawa and Jingu evaluated the angle between the direction

* Professor, Research Institute for Applied Mechanics, Kyushu University.
** Research Associate, Research Institute for Applied Mechanics, Kyushu University.
*** Associate Professor, Research Institute for Applied Mechanics, Kyushu University.

of ship's advance and the direction of wave pattern's propagation which was generated by a bow of a ship according to Hanaoka's theory[6], and estimated a critical circular frequency at which interference of tank wall began to affect motions of a ship[5]. Isshiki theoretically computed waves generated in a long canal with a periodic source[7]. One of the authors measured waves diffracted by a pile standing in a canal which is hydrodynamically equivalent to a row of infinitely many piles due to interference of tank walls and showed that his theory gives results in good agreement with the experimental ones[8].

The purpose of the present investigation in this paper is to estimate the hydrodynamic forces and moments acting on a ship body and the amplitudes of ship motions in a canal with a finite depth and a finite breadth for investigating differences between ship motions in a deep sea and a canal. We performed following three kinds of experiments in a water way constructed in our deep water tank for doing these experiments:

(i) Forced oscillating tests
(ii) Measurements of wave exciting forces
(iii) Measurements of ship motions in regular waves

We compared results in each experiment with theoretically calculated ones obtained by so-called "New Strip Theory" which does not take an interference effect of tank walls into account and derived some useful conclusions from consideration on the results.

2. Tank tests

Tank tests were performed in a canal which was especially constructed in the deep water tank of the Tsuyazaki Sea Safety Research Laboratory, the Research Institute for Applied Mechanics of Kyushu University.

2.1 Construction of canal

One way to make a shallow water condition in an existing deep water tank is to draw out water from a deep water tank and another is to build a false bottom in a deep water tank. In the former case we cannot use the existing experimental equipments to carry out forced oscillating test and to measure amplitudes of ship motions because of increasing distance between a surface of water and a towing carriage, and we have to make new experimental instruments. On the contrary, in the latter we can use the existing experimental instruments.

We adopted the latter plan and especially built a canal ($L\times B\times d=50$ m $\times 4$ m $\times 0.7$ m) in the deep water tank ($L\times B\times d=80$ m $\times 8$ m $\times 3.5$ m) as shown in Fig. 2.1. The water depth of the canal is variable from 0.2 m to 0.5 m by drawing or pouring water. And a wave making machine of flutter type was set at the end of the canal to generate waves with periods from 0.6 seconds to 3.0 seconds. The view of the canal and the wave making machine are shown in Photes 2.1~2.4.

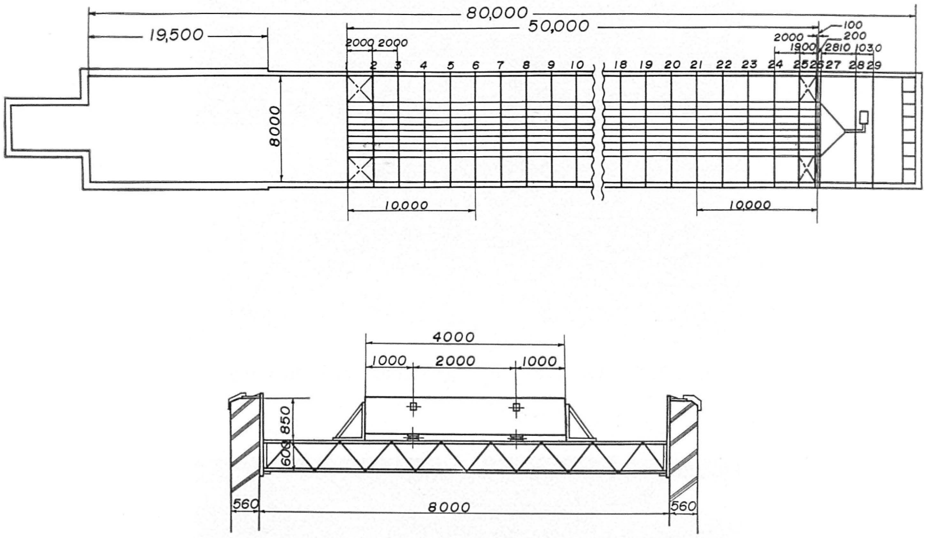

Fig. 2.1 General arrangement of canal

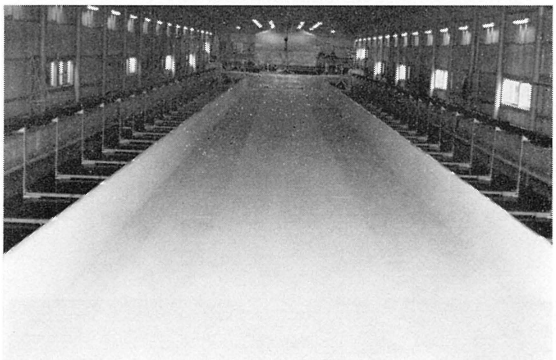

Photo 2.1 General view of canal before filling water

2.2 Methods and conditions of experiments

For the purpose of evaluating the effects of tank walls and water bottom on hydrodynamic forces acting on a ship and on ship motions in a canal with a finite depth and breadth for investigating differences between ship motions in deep water and in a canal, we performed three kinds of experiments mentioned in section 1 by using the ship model "Kasagisanmaru" for which hydrodynamic forces and response functions of motions in deep water had been studied. Experimental condition for the model is a full load condition and her principal dimensions are shown in Table 2.1. The experiment

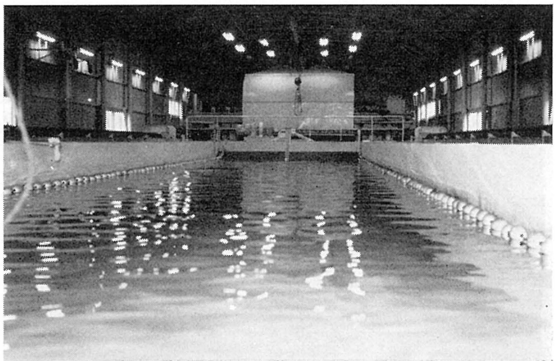

Photo 2.2 General view of canal with full water

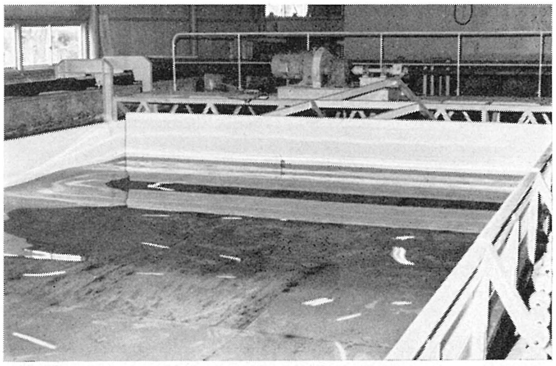

Photo 2.3 Wave making machine

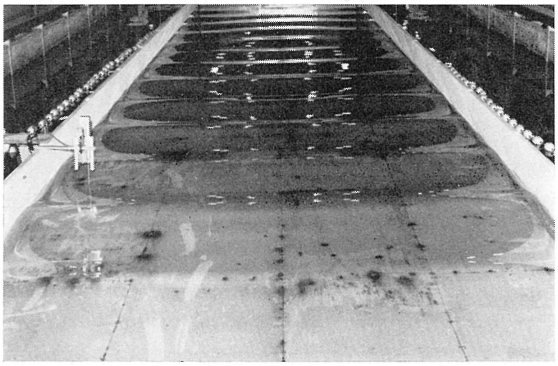

Photo 2.4 Regular wave generated in a canal

Table 2.1 Principal dimensions of ship model

Length between pependiculars	L_{pp} = 3.00 m
Breadth of ship	B = 0.493 m
Draft	T = 0.194 m
Displacement	Δ =231.1 Kg
Block coefficient	C_B = 0.8243
Metacentric height	$\overline{GM}$ = 0.045 m
Height of gravity from water line	$\overline{OG}$ = 0.040 m
Distance of gravity from midship	$\overline{⊠G}$ = 0.089 m
Radius of longitudinal gyration for yaw at forced yawing test	K_{yl} = 0.226 L_{pp}
Radius of transverse gyration for roll at forced rolling test	K_t = 0.305 B
Radius of longitudinal gyration for pitch at forced pitching test and ship motions	K_l = 0.210 L_{pp}
Radius of transverse gyration for roll at test of ship motions	K_t = 0.316 B
With bildge keel and rudder	
Without propeller	

Table 2.2 Conditions of forced oscillating tests

Mode	Amplitude	Ship Speed	Frequency	Depth of water
Forced Sway	y_A=2 cm	F_n=0, 0.1	$\frac{\omega^2}{g}T$=0.05 ~1.45 ω=1.59 ~8.55 (1/sec)	h/T=1.3, 1.8
Forced Roll	ϕ_A=5°, 10°, 12.5°, 15°	F_n=0, 0.075, 0.10		
Forced Yaw	ψ_A=1°, 2°	F_n=0, 0.10		
Forced Heave	Z_A=1.5 cm	F_n=0, 0.075, 0.10		
Forced Pitch	θ_A=1.43°			

Table 2.3 Conditions of measurement of wave exciting forces

Conditions	Ship Speed	Wave Frequency	Depth of water
Head sea (μ=180°)	F_n=0, 0.075, 0.10	$\frac{\omega_e^2}{g}T$=0.1 ~1.1 ω=2.24 ~7.5	h/T=1.3, 1.8
Bow sea (μ=135°)	F_n=0		
Beam sea (μ=90°)	F_n=0		

Table 2.4 Conditions of ship motions

Conditions	Ship Speed	Wave Frequency	Depth of water
Head sea (μ=180°)	F_n=0, 0.075, 0.1	$\frac{\omega_e^2}{g}T=0.1 \sim 1.1$	h/T=1.3, 1.8
Bow sea (μ=135°)	F_n=0	$\omega=2.24 \sim 7.5$	
Beam sea (μ= 90°)	F_n=0		

was carried out in a water depth 1.8 times and 1.3 times (water depth: h= 0.349 m, 0.252 m) as deep as draft of the model since it had been shown in the previous papers[10~12] that effects of water depth affected hydrodynamic forces on a ship and on ship motions in waves of water depth smaller than twice of a ship's draft. The experimental conditions are shown in Tables 2.2~2.4.

3. Equations of ship motions

As shown in Fig. 3.1, O'-$X_1Y_1Z_1$ is a coordinate system fixed in space with $O'X_1$ parallel to the canal, in which a regular wave progresses to the

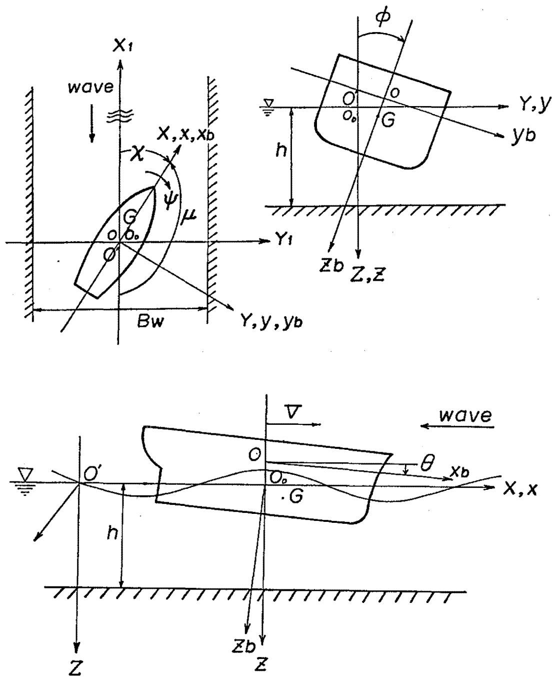

Fig. 3.1 Coordinate system

direction of X_1. Let O'-XYZ be another coordinate system fixed in space in which $O'X$ coincides with a centerline of a ship and directs forward, and let o-$x_b y_b z_b$ be a coordinate system fixed in a ship body, where o is the intersection of the centerline in a water plane of a ship and the midship. And let o_0-xyz be a coordinate system which is moving with a ship with a constant forward speed.

Suppose that a ship is making small motions in regular waves. The linear coupling equations for longitudinal motions and the linear coupling equations for lateral motions in regular waves can be expressed respectively as follows.

The equation for longitudinal motions:

$$(M+A_{11})\ddot{x}=F_{ye} \qquad \cdots\cdots\cdots\cdots(3.1)$$

$$\left.\begin{aligned}&(M+A_{33})\ddot{Z}+B_{33}\dot{Z}+C_{33}Z+A_{35}\ddot{\theta}+B_{35}\dot{\theta}+C_{35}\theta=F_{ze}\\&(J_{55}+A_{55})\ddot{\theta}+B_{55}\dot{\theta}+C_{55}\theta+A_{53}\ddot{Z}+B_{53}\dot{Z}+C_{53}Z=M_{\theta e}\end{aligned}\right]\cdots\cdots\ (3.2)$$

The equations for lateral motions:

$$\left.\begin{aligned}&(M+A_{22})\ddot{y}+B_{22}\dot{y}+A_{26}\ddot{\psi}+B_{26}\dot{\psi}+A_{24}\ddot{\phi}+B_{24}\dot{\phi}=F_{ye}\\&(J_{44}+A_{44})\ddot{\phi}+B_{44}\dot{\phi}+C_{44}\phi+A_{42}\ddot{y}+B_{42}\dot{y}+A_{46}\ddot{\psi}+B_{46}\dot{\psi}=M_{\phi e}\\&(J_{66}+A_{66})\ddot{\psi}+B_{66}\dot{\psi}+A_{64}\ddot{\phi}+B_{64}\dot{\phi}+A_{62}\ddot{y}+B_{62}\dot{y}=M_{\psi e}\end{aligned}\right]\quad(3.3)$$

The hydrodynamic coefficients A_{ij}, B_{ij} and C_{ij} in the left hand sides of the equations (3.1) (3.2) and (3.3) represent inertia terms, damping terms and restoring terms respectively. And the subscript of each coefficient denotes oscillating mode, $i=1$: surging mode, $i=2$: swaying mode, $i=3$: heaving mode, $i=4$: rolling mode, $i=5$: pitching mode and $i=6$: yawing mode. The hydrodynamic coefficients and the wave exciting force in the equations (3.1), (3.2) and (3.3) obtained by so-called "New Strip Method" are described in Appendix I.

4. Forced oscillating tests

Forced oscillating tests were performed in the canal shown in Fig. 2.1. The forced heaving test and the forced pitching test were carried out with a ship model set on the center of the canal parallel to it. The ship model was set perpendicular to the canal for the forced swaying, rolling and yawing oscillating tests with no forward speed in order to make interference effects of tank walls as small as possible. With forward speeds, however, the forced swaying, rolling and yawing tests were performed with a ship model set on parallel to the canal but away 0.17 m from the centerline of the canal because of convenience of forced oscilating machine mechanism.

We measured displacements of the ship model and hydrodynamic forces and moments acting on the ship body. These data were compiled by means of data recorder, and were analyzed with aid of Fourier analysis. Fourier component of frequency of ship oscillation were compared with the numerical results obtained by strip theory.

4.1 Analysis of forced oscillating tests

The coefficients in right hand side of equations (3.2) and (3.3) are derived respectively from amplitudes of hydrodynamic forces (F_{zA}, $M_{\theta A}$, F_{yA}, $M_{\phi A}$, $M_{\psi A}$) and phases (ε_z, ε_θ, ε_y, ε_ϕ, ε_ψ) measured in the forced oscillating test as follows.

$$\left.\begin{aligned} F_{ze} &= F_{zA} \sin(\omega t+\varepsilon_z) \\ M_{\theta e} &= M_{\theta A} \sin(\omega t+\varepsilon_\theta) \end{aligned}\right] \qquad \cdots\cdots\cdots\cdots (4.1)$$

$$\left.\begin{aligned} F_{ye} &= F_{yA} \sin(\omega t+\varepsilon_y) \\ M_{\phi e} &= M_{\phi A} \sin(\omega t+\varepsilon_\phi) \\ M_{\psi e} &= M_{\psi A} \sin(\omega t+\varepsilon_\psi) \end{aligned}\right] \qquad \cdots\cdots\cdots\cdots (4.2)$$

where

F_{zA} : amplitude of radiation force for heave,
$M_{\theta A}$: amplitude of radiation moment for pitch,
F_{yA} : amplitude of radiation force for sway,
$M_{\phi A}$: amplitude of radiation moment for roll,
$M_{\psi A}$: amplitude of radiation moment for yaw,
ε_z : phase lag between heaving displacement and radiation force of heaving,
ε_θ : phase lag between pitching displacement and radiation moment of pitching,
ε_y : phase lag between swaying displacement and radiation force of swaying,
ε_ϕ : phase lag between rolling displacement and radiation moment of rolling,
ε_ψ : phase lag between yawing displacement and radiation moment of yawing.

There exist following relationships among these coefficients of equations (3.2), (4.1), (3.3) and (4.2).[12]

(i) Forced heaving test

$$\left[\begin{aligned} M+A_{33} &= -\frac{F_{zA}\cos\varepsilon_z}{\omega^2 Z_A}+\frac{C_{33}}{\omega^2}, \\ B_{33} &= \frac{F_{zA}\sin\varepsilon_z}{\omega Z_A}. \end{aligned}\right. \qquad \cdots\cdots\cdots\cdots (4.3)$$

$$\left[\begin{aligned} &A_{53}-\frac{C_{53}}{\omega^2}=-\frac{M_{\theta A}\cos\varepsilon_\theta}{\omega^2 Z_A}, \\ &B_{53}=\frac{M_{\theta A}\sin\varepsilon_\theta}{\omega Z_A}. \end{aligned}\right. \qquad \cdots\cdots\cdots\cdots (4.4)$$

(ii) Forced pitching test

$$\left[\begin{aligned} &J_{55}+A_{55}=-\frac{M_{\theta A}\cos\varepsilon_\theta}{\omega^2\theta_A}+\frac{C_{55}}{\omega^2}, \\ &B_{55}=\frac{M_{\theta A}\sin\varepsilon_\theta}{\omega\theta_A}. \end{aligned}\right. \qquad \cdots\cdots\cdots\cdots (4.5)$$

$$\left[\begin{aligned} &A_{35}-\frac{C_{35}}{\omega^2}=-\frac{F_{zA}\cos\varepsilon_z}{\omega^2\theta_A}, \\ &B_{35}=\frac{F_{zA}\sin\varepsilon_z}{\omega\theta_A}. \end{aligned}\right. \qquad \cdots\cdots\cdots\cdots (4.6)$$

(iii) Forced swaying test

$$\left[\begin{aligned} &M+A_{22}=-\frac{F_{yA}\cos\varepsilon_y}{\omega^2 y_A}, \\ &B_{22}=\frac{F_{yA}\sin\varepsilon_y}{\omega y_A}. \end{aligned}\right. \qquad \cdots\cdots\cdots\cdots (4.7)$$

$$\left[\begin{aligned} &A_{42}=-\frac{M_{\phi A}\cos\varepsilon_\phi}{\omega^2 y_A}, \\ &B_{42}=\frac{M_{\phi A}\sin\varepsilon_\phi}{\omega y_A}. \end{aligned}\right. \qquad \cdots\cdots\cdots\cdots (4.8)$$

$$\left[\begin{aligned} &A_{62}=-\frac{M_{\psi A}\cos\varepsilon_\psi}{\omega^2 y_A}, \\ &B_{62}=\frac{M_{\psi A}\sin\varepsilon_\psi}{\omega y_A}. \end{aligned}\right. \qquad \cdots\cdots\cdots\cdots (4.9)$$

(iv) Forced rolling test

$$\left[\begin{aligned} &J_{44}+A_{44}=-\frac{M_{\phi A}\cos\varepsilon_\phi}{\omega^2\phi_A}+\frac{C_{44}}{\omega^2}, \\ &B_{44}=\frac{M_{\phi A}\sin\varepsilon_\phi}{\omega\phi_A}. \end{aligned}\right. \qquad \cdots\cdots\cdots\cdots (4.10)$$

$$\left[\begin{aligned} &A_{24}=-\frac{F_{yA}\cos\varepsilon_y}{\omega^2\phi_A}, \\ &B_{24}=\frac{F_{yA}\sin\varepsilon_y}{\omega\phi_A}. \end{aligned}\right. \qquad \cdots\cdots\cdots\cdots (4.11)$$

$$\begin{cases} A_{64} = -\dfrac{M_{\phi A}\cos\varepsilon_\phi}{\omega^2\phi_A}, \\ B_{64} = \dfrac{M_{\phi A}\sin\varepsilon_\phi}{\omega\phi_A}. \end{cases} \qquad \cdots\cdots\cdots\cdots(4.12)$$

(v) Forced yawing test

$$\begin{cases} J_{66}+A_{66} = -\dfrac{M_{\psi A}\cos\varepsilon_\psi}{\omega^2\psi_A}, \\ B_{66} = \dfrac{M_{\psi A}\sin\varepsilon_\psi}{\omega\psi_A}. \end{cases} \qquad \cdots\cdots\cdots\cdots(4.13)$$

$$\begin{cases} A_{26} = -\dfrac{F_{\eta A}\cos\varepsilon_\eta}{\omega^2\psi_A}, \\ B_{26} = \dfrac{F_{\eta A}\sin\varepsilon_\eta}{\omega\psi_A}. \end{cases} \qquad \cdots\cdots\cdots\cdots(4.14)$$

$$\begin{cases} A_{46} = -\dfrac{M_{\phi A}\cos\varepsilon_\phi}{\omega^2\psi_A}, \\ B_{46} = \dfrac{M_{\phi A}\sin\varepsilon_\phi}{\omega\psi_A}. \end{cases} \qquad \cdots\cdots\cdots\cdots(4.15)$$

As shown in the above relationships, the coefficients of equations (3.2) and (3.3) can be obtained by performing the five kinds of the forced oscillating tests (heaving, pitching, swaying, rolling and yawing).

4.2 Expression of experimental results

Non-dimensional coefficients of A_{ij} and B_{ij} obtained in 4.1 section are shown as follows:

(i) Coefficients obtained by forced heaving test

$$\hat{M}+\hat{A}_{33} = \frac{M+A_{33}}{\rho L^3}, \qquad \hat{B}_{33} = \frac{B_{33}}{\rho L^3}\sqrt{B/2g},$$

$$\hat{A}_{53} = \frac{A_{53}-C_{53}/\omega^2}{\rho L^4}, \qquad \hat{B}_{53} = \frac{B_{53}}{\rho L^4}\sqrt{B/2g}.$$

(ii) Coefficients obtained by forced pitching test

$$\hat{J}_{55}+\hat{A}_{55} = \frac{J_{55}+A_{55}}{\rho L^5}, \qquad \hat{B}_{55} = \frac{B_{55}}{\rho L^5}\sqrt{B/2g},$$

$$\hat{A}_{35} = \frac{A_{35}-C_{35}/\omega^2}{\rho L^4}, \qquad \hat{B}_{35} = \frac{B_{35}}{\rho L^4}\sqrt{B/2g}.$$

(iii) Coefficients obtained by forced swaying test

$$\hat{M}+\hat{A}_{22} = \frac{M+A_{22}}{\rho \varDelta}, \qquad \hat{B}_{22} = \frac{B_{22}}{\rho \varDelta}\sqrt{B/2g},$$

$$\hat{A}_{42}=\frac{A_{42}}{\rho\Delta B}, \qquad \hat{B}_{42}=\frac{B_{42}}{\rho\Delta B}\sqrt{B/2g},$$

$$\hat{A}_{62}=\frac{A_{62}}{\rho\Delta L}, \qquad \hat{B}_{62}=\frac{B_{62}}{\rho\Delta L}\sqrt{B/2g}.$$

(iv) Coefficients obtained by forced rolling test

$$\hat{J}_{44}+\hat{A}_{44}=\frac{J_{44}+A_{44}}{\rho\Delta B^2}, \qquad \hat{B}_{44}=\frac{B_{44}}{\rho\Delta B^2}\sqrt{B/2g},$$

$$\hat{A}_{24}=\frac{A_{24}}{\rho\Delta B}, \qquad \hat{B}_{24}=\frac{B_{24}}{\rho\Delta B}\sqrt{B/2g},$$

$$\hat{A}_{64}=\frac{A_{64}}{\rho\Delta LB}, \qquad \hat{B}_{64}=\frac{B_{64}}{\rho\Delta LB}\sqrt{B/2g}.$$

(v) Coefficients obtained by forced yawing test

$$\hat{J}_{66}+\hat{A}_{66}=\frac{J_{66}+A_{66}}{\rho\Delta L^2}, \qquad \hat{B}_{66}=\frac{B_{66}}{\rho\Delta L^2}\sqrt{B/2g},$$

$$\hat{A}_{26}=\frac{A_{26}}{\rho\Delta L}, \qquad \hat{B}_{26}=\frac{B_{26}}{\rho\Delta L}\sqrt{B/2g},$$

$$\hat{A}_{46}=\frac{A_{46}}{\rho\Delta LB}, \qquad \hat{B}_{46}=\frac{B_{46}}{\rho\Delta LB}\sqrt{B/2g}.$$

where

L : length of ship,
B : breadth of ship,
M : mass of ship ($=\rho\Delta$),
Δ : displacement of ship,
J_{ii} : mass moment of inertia of ship for the i-th mode,
ρ : density of water,
g : gravitational acceleration.

4.3 Comparison of theoretical predictions with experimental results

The comparisons of experimental results with theoretical ones obtained by new strip theory which does not take interference effects of tank walls into account are shown in Figs. 4.1~4.40. In this paper all theoretical computations are done with making use of new strip method which does not take effects of tank walls into account but effects of finite water depth.

4.3.1 Coefficients for heaving and pitching motions

(i) Inertia terms: $\hat{A}_{33}$, $\hat{A}_{55}$

Measured values of $\hat{A}_{33}$ and $\hat{A}_{55}$ without a forward speed ($F_n=0$) show hump and hollow variations around theoretical curves. The non-dimensional frequencies $\left(\frac{\omega^2}{g}T\right)$ at which humps and hollows of experimental values appear are shown in Table 4.1.

When a forward speed is not zero ($F_n=0.10$), experimental values of $\hat{A}_{33}$ and $\hat{A}_{55}$ do not show a hump and a hollow variation, and are in agree-

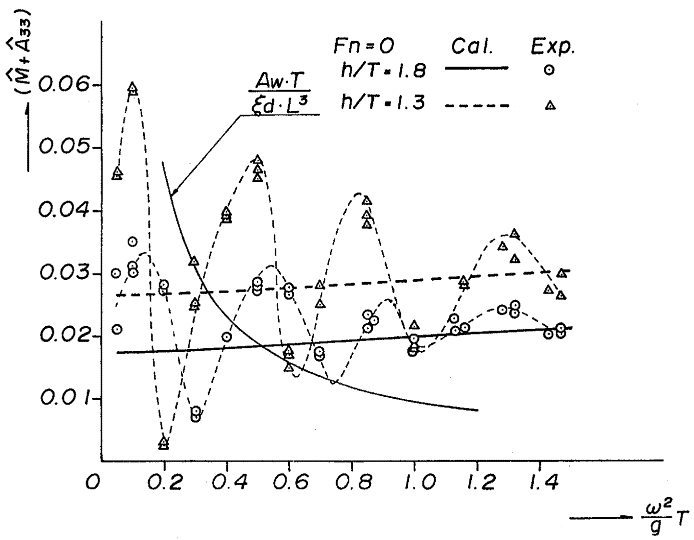

Fig. 4.1 $\hat{M}+\hat{A}_{33}$: Virtual mass coeff. for heave at $F_n=0$

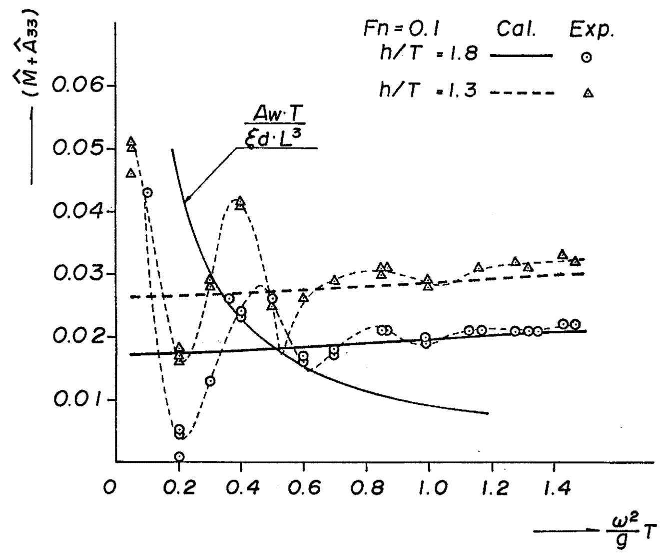

Fig. 4.2 $\hat{M}+\hat{A}_{33}$: Virtual mass coeff. for heave at $F_n=0.10$

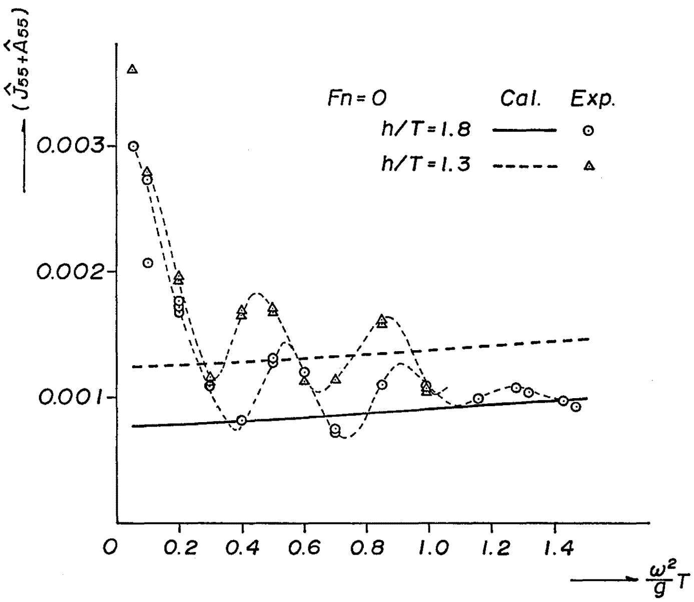

Fig. 4.3 $\hat{J}_{55}+\hat{A}_{55}$: Virtual mass moment of inertia coeff. for pitch at $F_n=0$

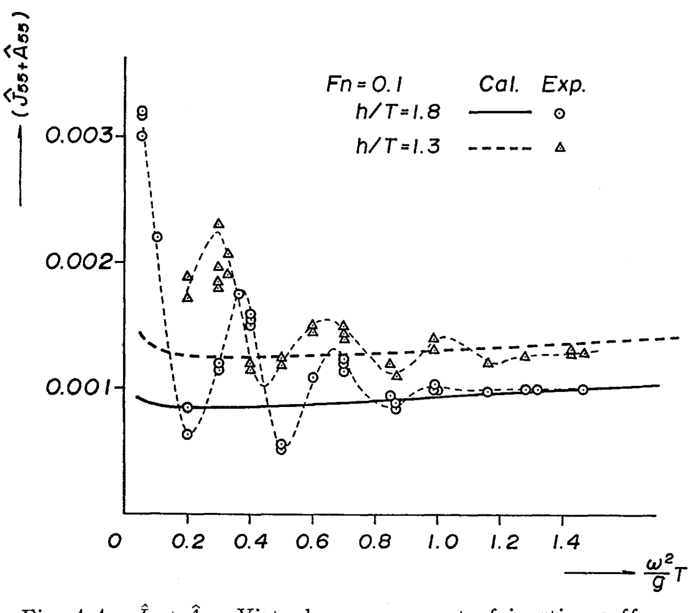

Fig. 4.4 $\hat{J}_{55}+\hat{A}_{55}$: Virtual mass moment of inertia coeff. for pitch at $F_n=0.10$

ment with the theoretical ones in high frequency $\left(\frac{\omega^2}{g}T>1.1\right)$. But in low frequency $\left(\frac{\omega^2}{g}T<1.1\right)$, measured values of $\hat{A}_{33}$ take minimum or maximum value at the frequency shown in Table 4.1 (Fig. 4.2), while humps of $\hat{A}_{55}$ with forward speeds appear at the same frequencies as hollows of $\hat{A}_{55}$ without a forward speed appear as shown in Table 4.1 (Fig. 4.4). These humps and hollows appearing in experimental results are considered to be interference effects of tank walls due to reflection from tank walls of waves generated by the motions of the ship.

(ii) Damping terms: $\hat{B}_{33}$, $\hat{B}_{55}$

Without a forward speed, experimental values of $\hat{B}_{33}$ and $\hat{B}_{55}$ show large humps and hollows and take maximum values or minimum ones at frequencies shown in Table 4.2. The minimum values of $\hat{B}_{33}$ and $\hat{B}_{55}$ in low frequencies are much smaller than theoretical values, while in high frequencies they are larger than theoretical ones (Fig. 4.5). Comparing Table 4.1 with Table 4.2, we can see the maximum values of $\hat{A}_{33}$ and $\hat{B}_{33}$ appear at almost the same frequencies. The same tendencies as those in heaving mode appear also in pitching mode, but those in pitching mode are not so explicit as those in heaving mode.

With a forward speed ($F_n=0.10$), the humps and hollows of experimental values $\hat{B}_{33}$ appear at the frequencies as shown in Table 4.2 (Fig. 4.6). Humps of experimental values $\hat{B}_{55}$ with a forward speed appear at the same frequencies as hollows of $\hat{B}_{55}$ without a forward speed appear as shown in Table 4.2.

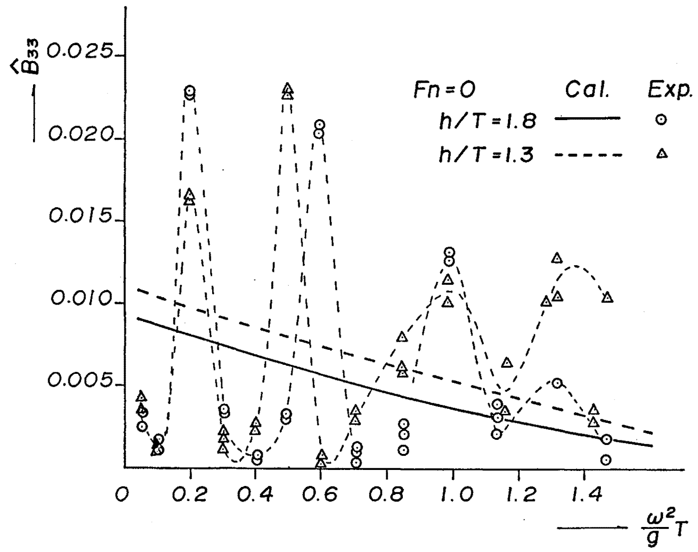

Fig. 4.5 $\hat{B}_{33}$: Damping force coeff. heave at $F_n=0$

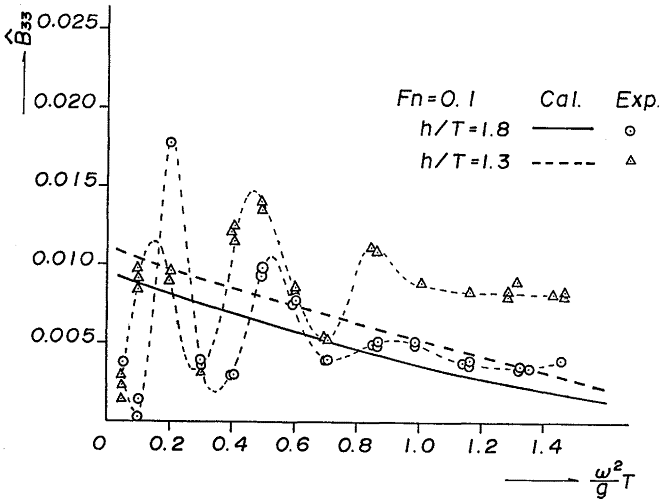

Fig. 4.6 $\hat{B}_{33}$: Damping force coeff. for heave at $F_n=0.10$

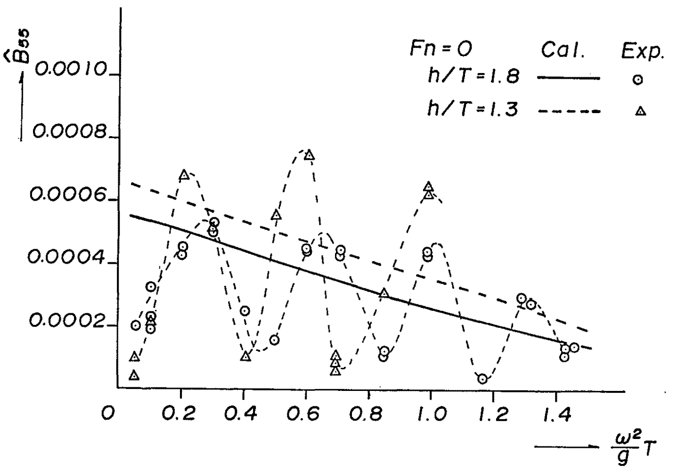

Fig. 4.7 $\hat{B}_{55}$ Damping moment coeff. for pitch at $F_n=0$

(iii) Cross coupling terms: $\hat{A}_{53}$, $\hat{A}_{35}$; $\hat{B}_{53}$, $\hat{B}_{35}$

Experimental values of $\hat{A}_{53}$, $\hat{A}_{35}$, $\hat{B}_{53}$ and $\hat{B}_{35}$ without a forward speed fluctuate around the mean line given by theoretical calculations respectively at overall experimental frequencies. However these experimental values almost satisfy the symmetric relationships ($\hat{A}_{53}=\hat{A}_{35}$, $\hat{B}_{53}=\hat{B}_{35}$) as shown in Figs. 4.9～4.12.

In case of a forward speed ($F_n=0.10$), experimental values of $\hat{A}_{53}$, $\hat{A}_{35}$, B_{53} and $\hat{B}_{35}$ also fluctuated around the mean line given by new strip method

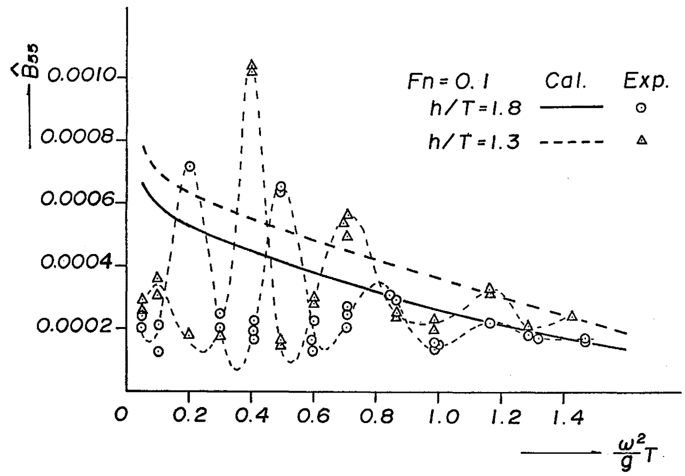

Fig. 4.8 $\hat{B}_{55}$: Damping moment coeff. for pitch at F_n =0.10

Table 4.1 Frequency $\left(\frac{\omega^2}{g}T\right)$ of humps and hollows in $\hat{A}_{33}$ and $\hat{A}_{55}$ at $F_n=0$

		$h/T=1.3$	$h/T=1.8$
		$\frac{\omega^2}{g}T$	$\frac{\omega^2}{g}T$
$\hat{A}_{33}$	Freq. of humps	0.1, 0.4~0.5, 0.85, 1.3	0.2, 0.5~0.6, 0.85, 1.3
	Freq. of hollows	0.2, 0.6, 1.0	0.3, 0.7, 1.0
$\hat{A}_{55}$	Freq. of humps	0.4, 0.5, 0.85	0.5~0.6, 0.85, 1.3
	Freq. of hollows	0.3, 0.6~0.7, 1.0	0.4, 0.7

Table 4.2 Frequencies $\left(\frac{\omega^2}{g}T\right)$ when humps and hollows appear in $\hat{B}_{33}$ and $\hat{B}_{55}$ at Fn=0

		$h/T=1.3$	$h/T=1.8$
		$\frac{\omega^2}{g}T$	$\frac{\omega^2}{g}T$
$\hat{B}_{33}$	Freq. of humps	0.2, 0.5, 1.0, 1.35	0.2, 0.6, 1.0, 1.3
	Freq. of hollows	0.35, 0.6, 1.15	0.4, 0.7, 0.8, 1.1
$\hat{B}_{55}$	Freq. of humps	0.2, 0.6, 1.0	0.3, 0.6, 0.7, 1.0, 1.3
	Freq. of hollows	0.4, 0.7	0.45, 0.85, 1.15

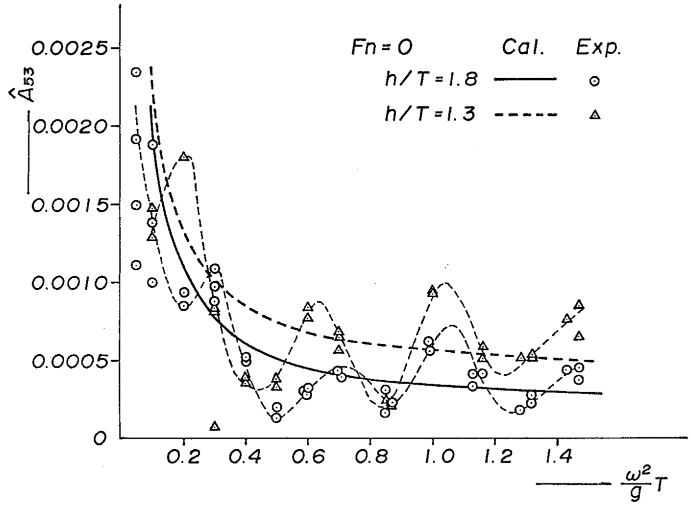

Fig. 4.9 $\hat{A}_{53}$: Coupling moment coeff. of heave into pitch at $F_n=0$

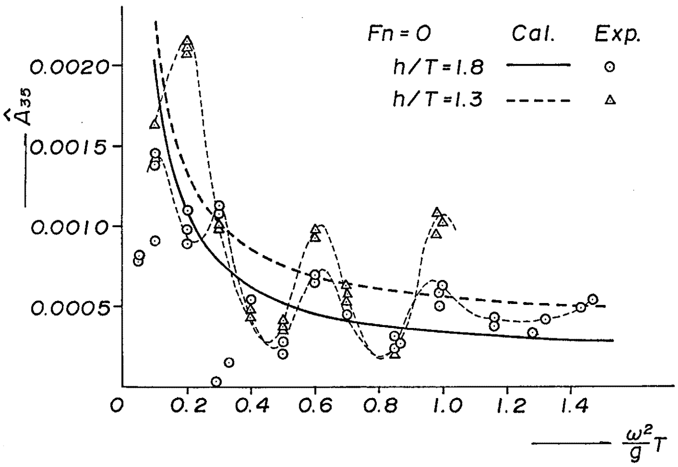

Fig. 4.10 $\hat{A}_{35}$: Coupling force coeff. of pitch into heave at $F_n=0$

and show hump and hollow variations at almost the same frequency as those without a forward speed (Figs. 4.13~4.16).

4.3.2 Coefficients for swaying, yawing and rolling

(i) No forward speed

Radiation forces ($\hat{A}_{22}$, $\hat{B}_{22}$), wave exciting force and response curve for swaying mode without a forward speed are shown in Figs. 4.17~4.20. It is clear that when the ship model is set in the tank so that her center line

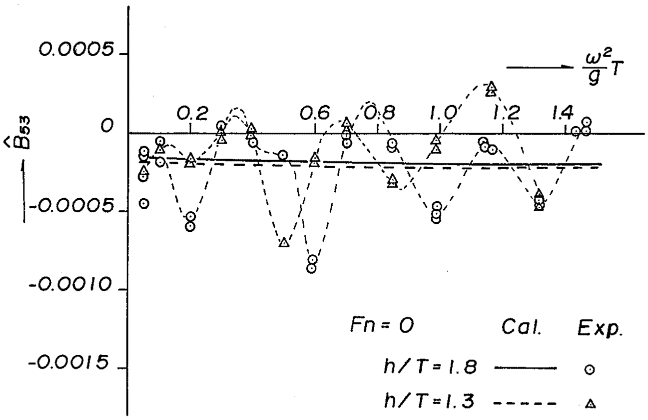

Fig. 4.11 $\hat{B}_{53}$: Coupling force coeff. of heave into pitch at $F_n=0$

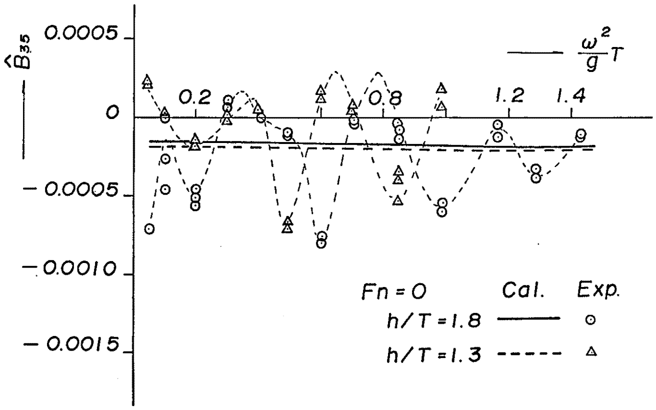

Fig. 4.12 $\hat{B}_{35}$: Coupling moment coeff. of pitch into heave at $F_n=0$

is perpendicular to the tank wall, the hydrodynamic forces and moments on the ship model and the amplitudes of the ship motions are scarcely affected by interference effects of tank walls. Consequently the results obtained when the ship model is at this position are not shown hereafter, and the results alone for the ship model set with her centerline parallel to the tank wall are described in this paper.

(ii) Principal terms for swaying: $\hat{A}_{22}$, $\hat{B}_{22}$

Experimental values of $\hat{A}_{22}$ and $\hat{B}_{22}$ fluctuate around their theoretical values as shown in Fig. 4.21 and Fig. 4.22. These humps and hollows appear at the frequencies $\left(\frac{\omega^2}{g}T\right)$ shown in Table 4.3.

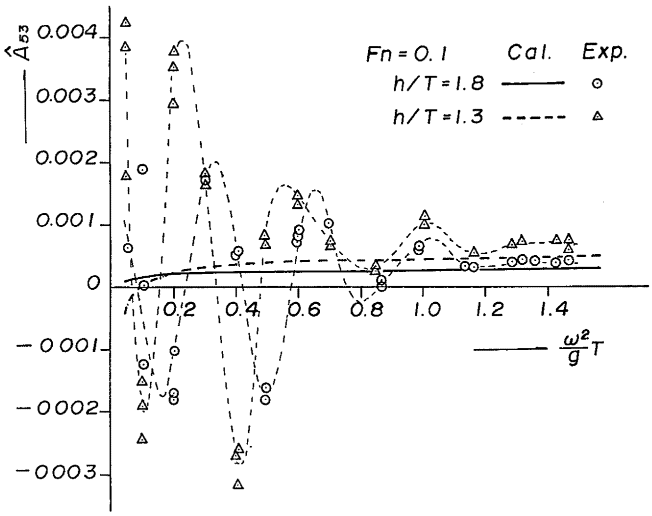

Fig. 4.13 $\hat{A}_{53}$: Coupling moment coeff. of heave into pitch at $F_n=0.10$

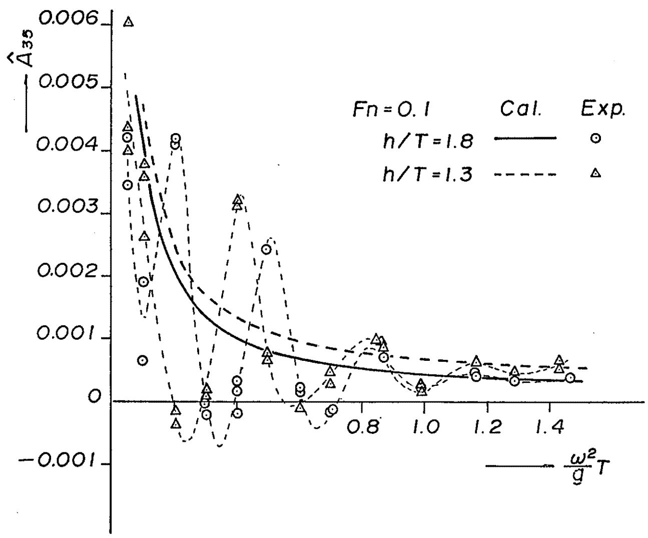

Fig. 4.14 $\hat{A}_{35}$: Coupling force coeff. of pitch into heave at $F_n=0.10$

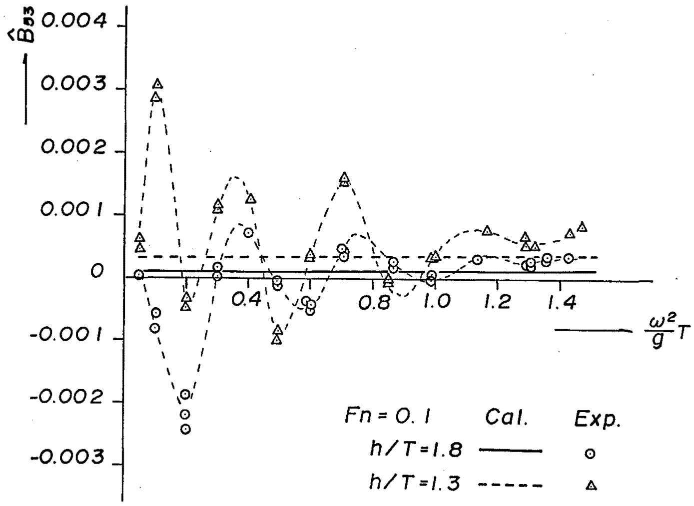

Fig. 4.15 $\hat{B}_{53}$: Coupling force coeff. of heave into pitch at $F_n=0.1$

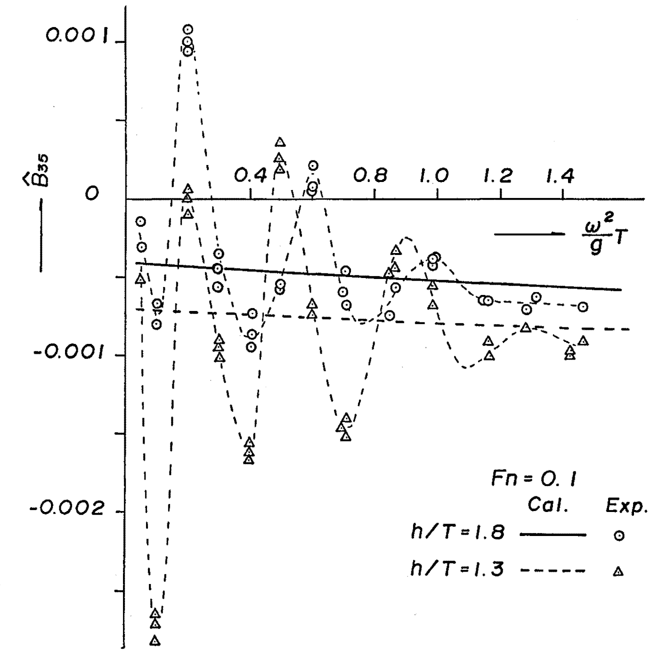

Fig. 4.16 $\hat{B}_{35}$: Coupling moment coeff. of pitch into heave at $F_n=0.1$

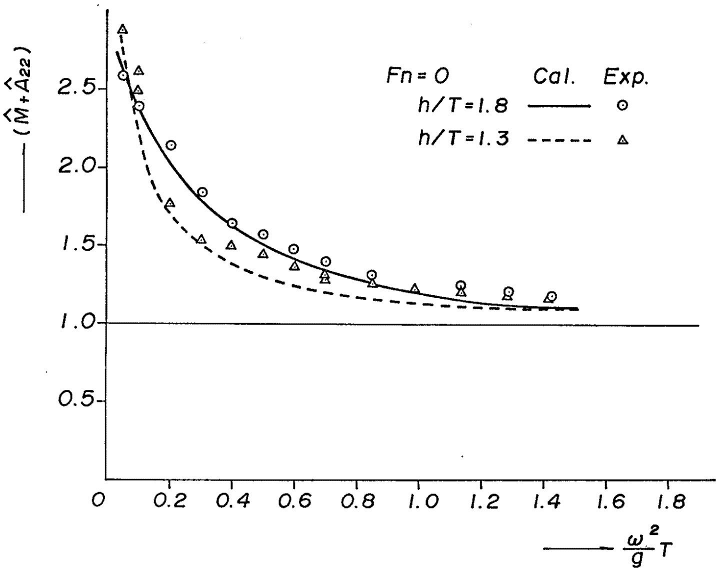

Fig. 4.17 $\hat{M}+\hat{A}_{22}$: Virtual mass coeff. for sway at $F_n=0$

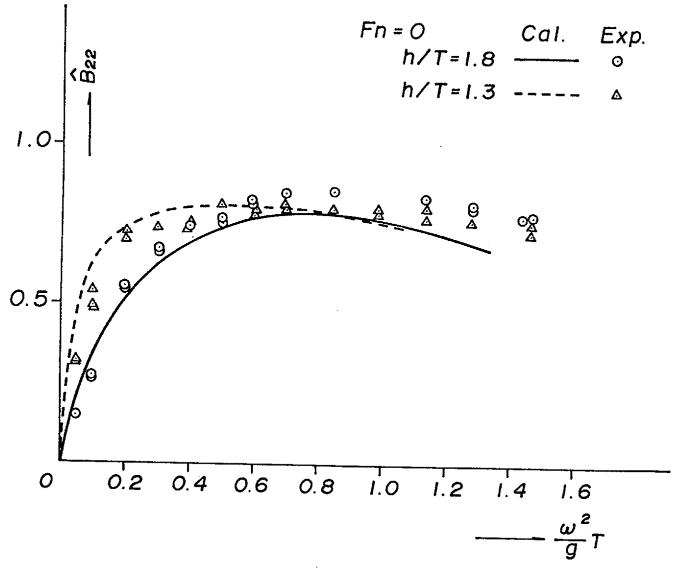

Fig. 4.18 $\hat{B}_{22}$: Damping coeff. for sway at $F_n=0$

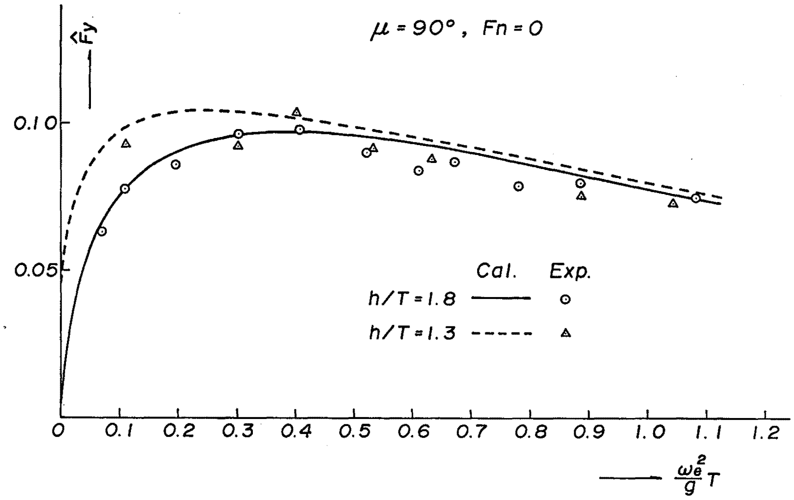

Fig. 4.19 $\hat{F}_y$: Wave exciting force for sway at $F_n=0$ in beam sea condition

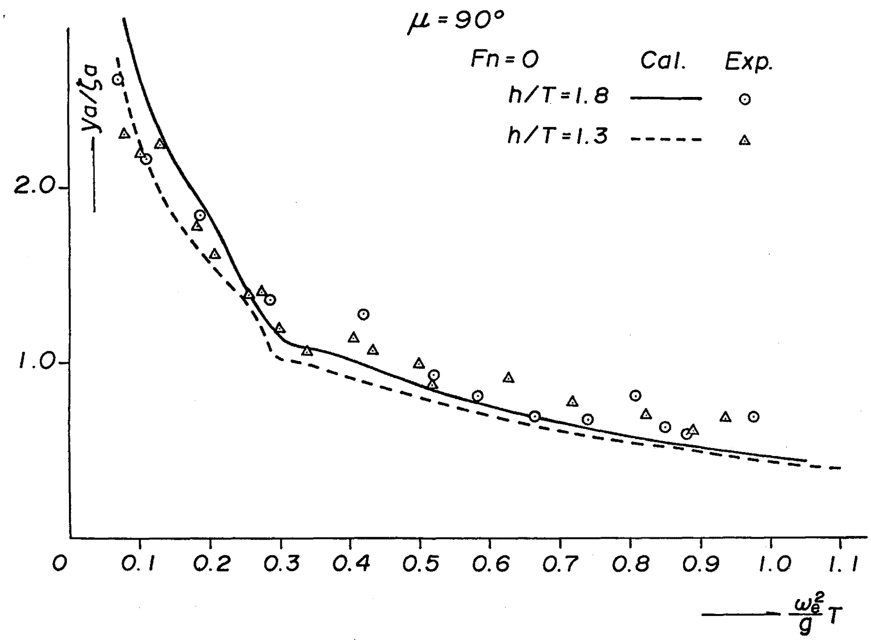

Fig. 4.20 Swaying amplitude at $F_n=0$ in beam sea condition

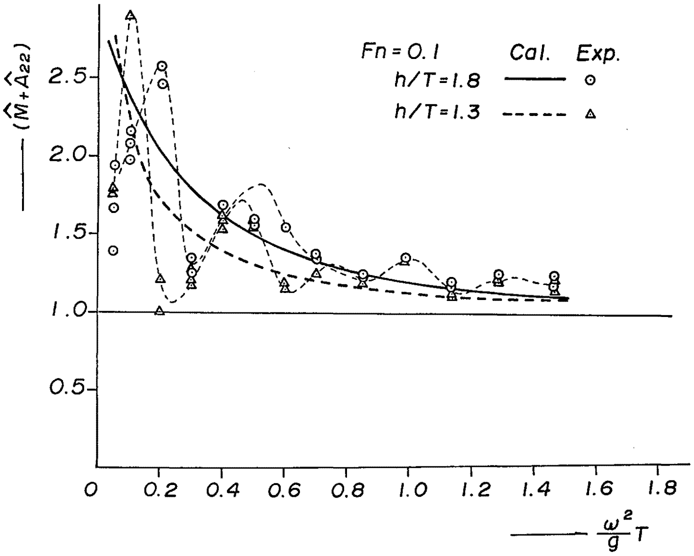

Fig. 4.21 $\hat{M}+\hat{A}_{22}$: Virtual mass coeff. for sway at $F_n=0.10$

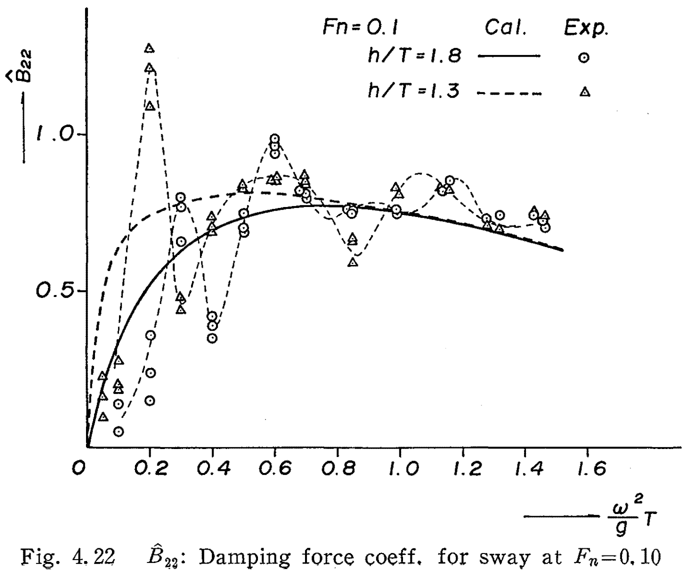

Fig. 4.22 $\hat{B}_{22}$: Damping force coeff. for sway at $F_n=0.10$

Table 4.3 Frequencies $\left(\frac{\omega^2}{g}T\right)$ when humps and hollows appear in $\hat{A}_{22}$ and $\hat{B}_{22}$

		$h/T=1.3$	$h/T=1.8$
		$\frac{\omega^2}{g}T$	$\frac{\omega^2}{g}T$
$\hat{A}_{22}$	Freq. of humps	0.1, 0.4∼0.5, 1.0	0.2, 0.4∼0.5, 1.0
	Freq. of hollows	0.2∼0.3, 0.6, 1.1	0.3, 0.6, 1.1
$\hat{B}_{22}$	Freq. of humps	0.2, 0.6, 1.1	0.3, 0.6 1.1
	Freq. of hollows	0.3, 0.85	0.4, 1.0

From the above table, it is seen that the values of $\hat{A}_{22}$ are above the theoretical values at the frequencies when the values of $\hat{B}_{22}$ are under the theoretical ones and ones of $\hat{A}_{22}$ are under the theoretical ones at the frequencies when the values of $\hat{B}_{22}$ are above the theoretical ones.

(iii) Principal terms for rolling: $\hat{A}_{44}$, $\hat{B}_{44}$

The experimental values of virtual mass moment of inertia for roll $\hat{A}_{44}$ are scarcely affected by interference effects of tank walls. It is because the wave amplitudes generated by rolling motion are smaller than those generated by other mode and the amplitudes of reflection wave from the tank walls consequently are very small. This tendency is different from that of other modes.

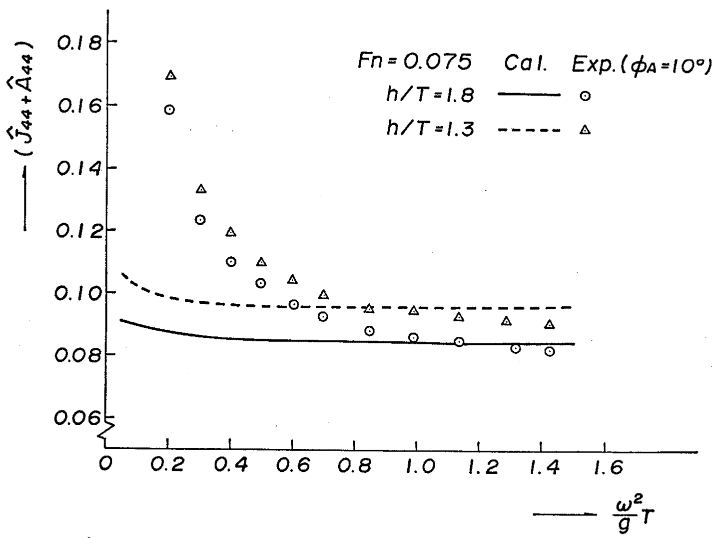

Fig. 4.23 $\hat{J}_{44}+\hat{A}_{44}$: Virtual mass moment of inertia coeff. for roll at $F_n=0.075$

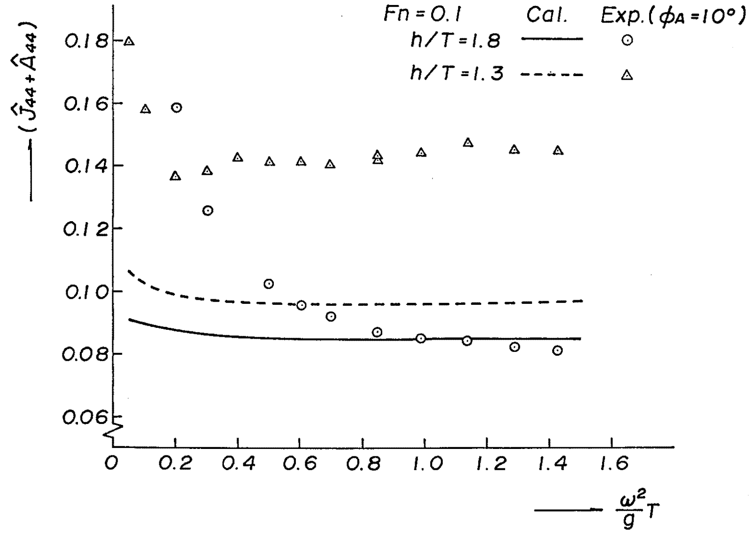

Fig. 4.24 $\hat{J}_{44}+\hat{A}_{44}$: Virtual mass moment of inertia coeff. for roll at F_n=0.10

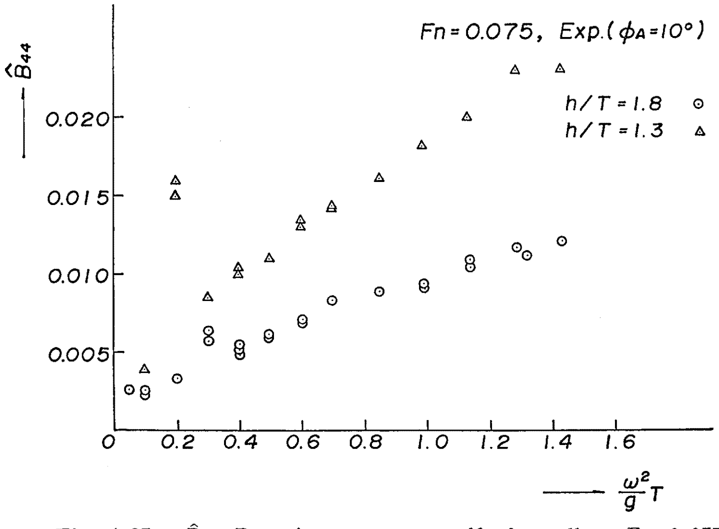

Fig. 4.25 $\hat{B}_{44}$: Damping moment coeff. for roll at F_n=0.075

Experimental values of $\hat{A}_{44}$ are in agreement with theoretical ones in high frequencies, while in low frequencies the experimental values become larger than the theoretical ones (Figs. 4.23, 4.24). As the water depth becomes more shallow and the forward speed of ship becomes larger, the experimental values of the virtual mass moment of inertia $(\hat{J}_{44}+\hat{A}_{44})$ for

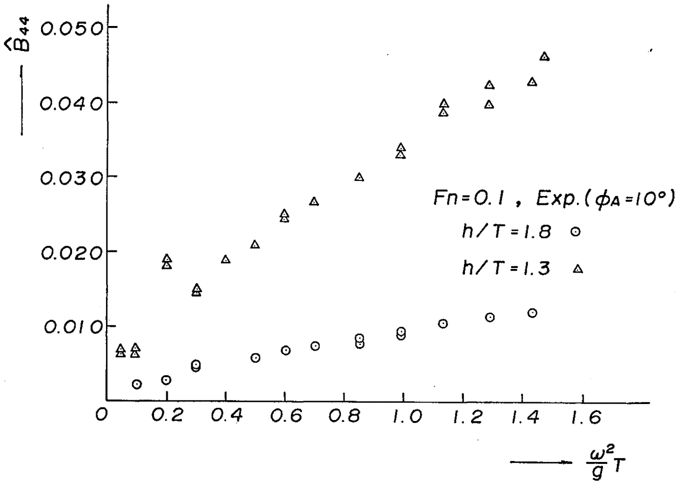

Fig. 4.26 $\hat{B}_{44}$: Damping moment coeff. for roll at $F_n=0.10$

Table 4.4 Frequencies $\left(\frac{\omega^2}{g}T\right)$ when humps and hollows appear in $\hat{B}_{44}$

	$h/T=1.3$	$h/T=1.8$
	$\frac{\omega^2}{g}T$	$\frac{\omega^2}{g}T$
Fn=0.075	0.2	0.3
Fn=0.10	0.2	0.3

rolling mode become larger than theoretical ones at overall frequencies where experiment were done (Fig. 4.24).

Experimental values of damping moment for rolling $\hat{B}_{44}$ have only one hump due to interference effects of tank walls at the frequency shown in Table 4.4 and are scarcely affected by interference effects of tank walls in other frequencies as in the case of $\hat{A}_{44}$.

(iv) Principal terms for yawing: $\hat{A}_{66}$, $\hat{B}_{66}$

Experimental values of $\hat{A}_{66}$ and $\hat{B}_{66}$ fluctuate around their theoretical values respectively as shown in Fig. 4.27 and Fig. 4.28. These humps and hollows appear at the frequencies $\left(\frac{\omega^2}{g}T\right)$ shown in Table 4.5.

From the above table it is seen that the tendencies of humps and hollows for $\hat{A}_{66}$ and $\hat{B}_{66}$ are similar to those of $\hat{A}_{22}$ and $\hat{B}_{22}$ (Figs. 4.21, 4.22).

(v) Cross coupling terms: $\hat{A}_{ij}$, $\hat{B}_{ij}$, $\hat{A}_{ji}$, $\hat{B}_{ji}$

$\hat{A}_{42}$, $\hat{B}_{42}$, $\hat{A}_{24}$, $\hat{B}_{24}$

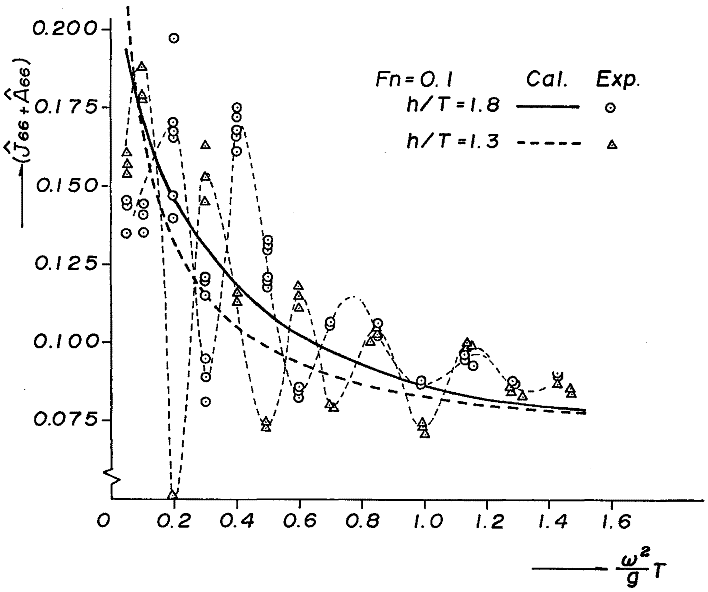

Fig. 4.27 $\hat{J}_{66}+\hat{A}_{66}$: Virtual mass moment of inertia coeff. for yaw at $F_n=0.10$

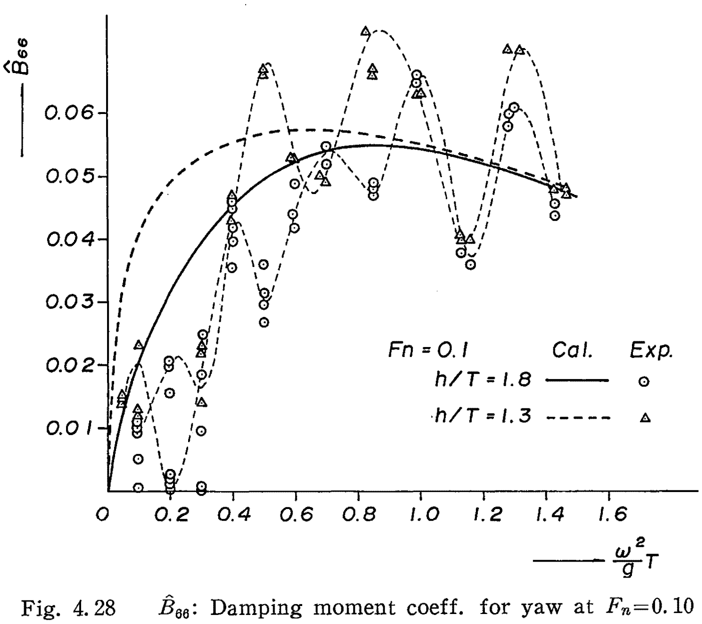

Fig. 4.28 $\hat{B}_{66}$: Damping moment coeff. for yaw at $F_n=0.10$

Table 4.5 Frequencies $\left(\frac{\omega^2}{g}T\right)$ when humps and hollows appear in $\hat{A}_{66}$ and $\hat{B}_{66}$

		$h/T=1.3$	$h/T=1.8$
		$\frac{\omega^2}{g}T$	$\frac{\omega^2}{g}T$
$\hat{A}_{66}$	Freq. of humps	0.1, 0.3, 0.6, 0.85, 1.15	0.2, 0.4, 0.8, 1.15
	Freq. of hollows	0.2, 0.5, 0.7, 1.0	0.3, 0.6, 1.0
$\hat{B}_{66}$	Freq. of humps	0.5, 0.85, 1.3	0.4, 0.7, 1.0, 1.3
	Freq. of hollows	0.2, 0.7, 1.15	0.5, 0.85, 1.15

The subscript $i=2$, $j=4$ of each coefficient denotes coupling term from rolling mode into swaying mode or from swaying mode into rolling mode. Experimental values of $\hat{A}_{42}$ and $\hat{B}_{42}$ fluctuate and reach to the maximum or minimum value at the same frequencies as $\hat{A}_{22}$ and $\hat{B}_{22}$ do as shown in Table 4.3 (Fig. 4.29, 4.30). While interference effects of tank walls on $\hat{A}_{24}$ and $\hat{B}_{24}$ are not so strong as ones on $\hat{A}_{42}$ and $\hat{B}_{42}$ (Fig. 4.31, 4.32), because the wave amplitudes generated by rolling motion are smaller than those due to swaying motion.

$\hat{A}_{62}$, $\hat{B}_{62}$, $\hat{A}_{26}$, $\hat{B}_{26}$

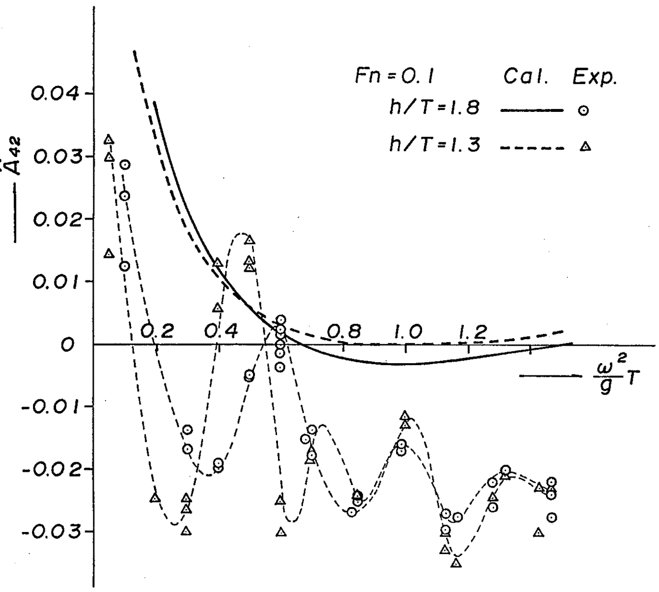

Fig. 4.29 $\hat{A}_{42}$: Coupling moment coeff. of sway into roll at $F_n=0.10$

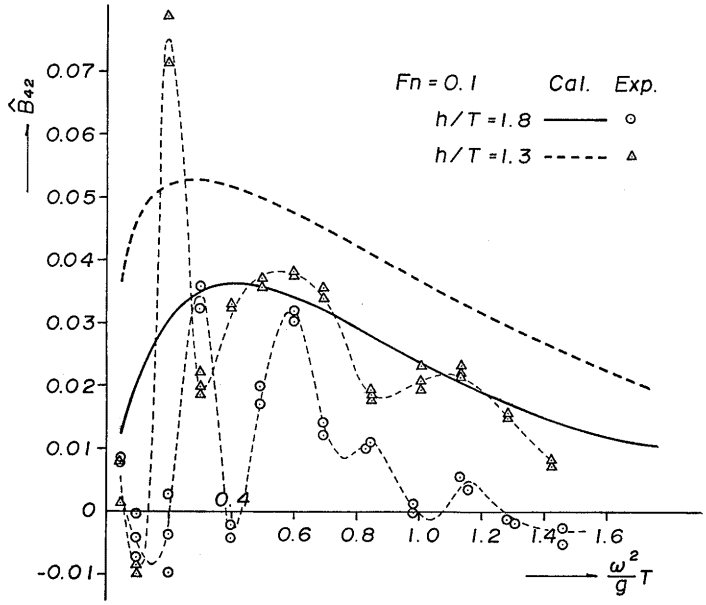

Fig. 4.30 $\hat{B}_{42}$: Coupling moment coeff. of sway into roll at $F_n=0.10$

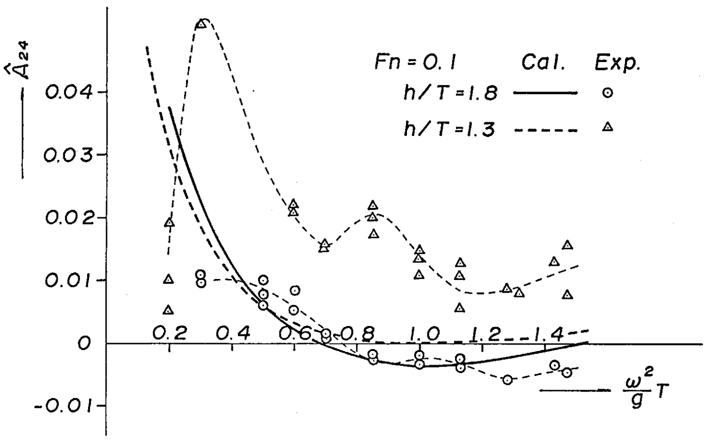

Fig. 4.31 $\hat{A}_{24}$: Coupling force coeff. of roll into sway at $F_n=0.10$

The subscript $i=2$, $j=6$ of each coefficient denotes coupling term between swaying and yawing mode. Experimental values of $\hat{A}_{ij}$, $\hat{B}_{ij}$ fluctuate around the theoretical ones obtained by new strip method (Figs. 4.33~4.36). It is seen from these figures that humps of $\hat{A}_{62}$ and $\hat{B}_{62}$ appear at the same frequencies as hollows of $\hat{A}_{26}$ and $\hat{B}_{26}$ appear respectively, while hollows of $\hat{A}_{62}$ and $\hat{B}_{62}$ appear at the same frequencies as humps of $\hat{A}_{26}$ and $\hat{B}_{26}$ appear

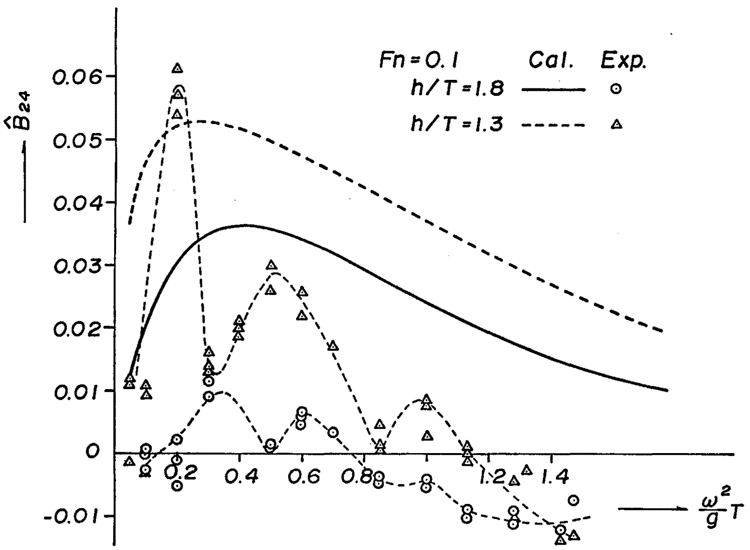

Fig. 4.32 $\hat{B}_{24}$: Coupling force coeff. of roll into sway at F_n=0.10

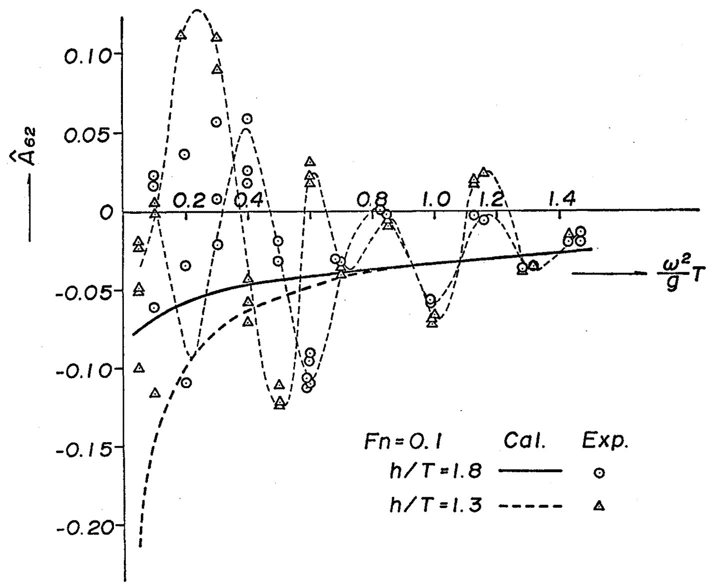

Fig. 4.33 $\hat{A}_{62}$: Coupling moment coeff. of sway into yaw at F_n=0.10

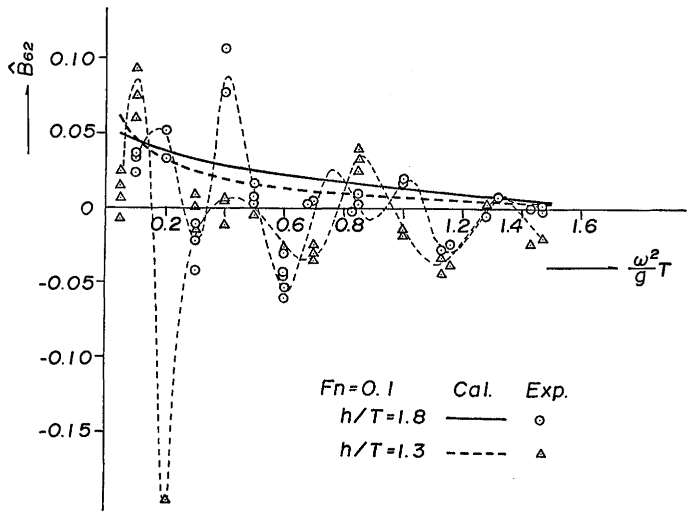

Fig. 4.34 $\hat{B}_{62}$: Coupling moment coeff. of sway into yaw at $F_n=0.10$

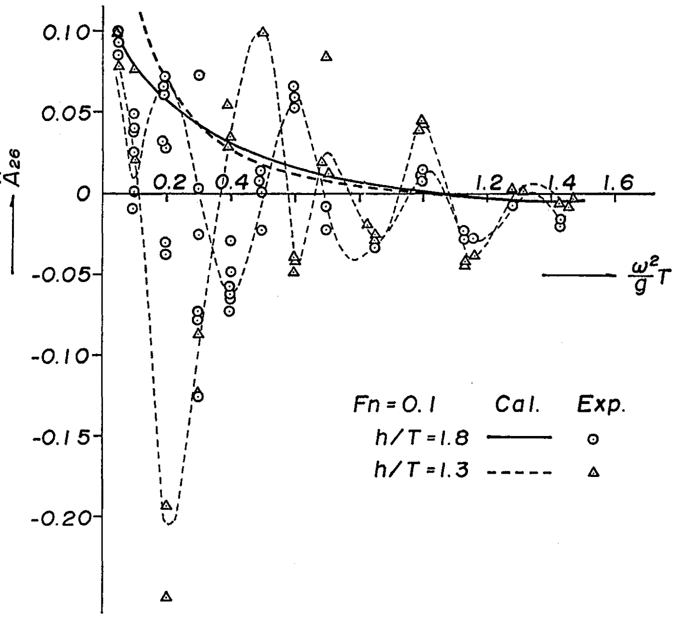

Fig. 4.35 $\hat{A}_{26}$: Coupling force coeff. of yaw into sway at $F_n=0.10$

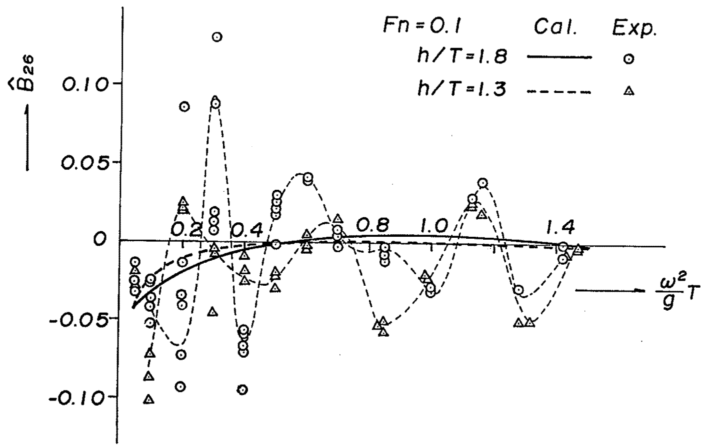

Fig. 4.36 $\hat{B}_{26}$: Coupling force coeff. of yaw into sway at $F_n=0.10$

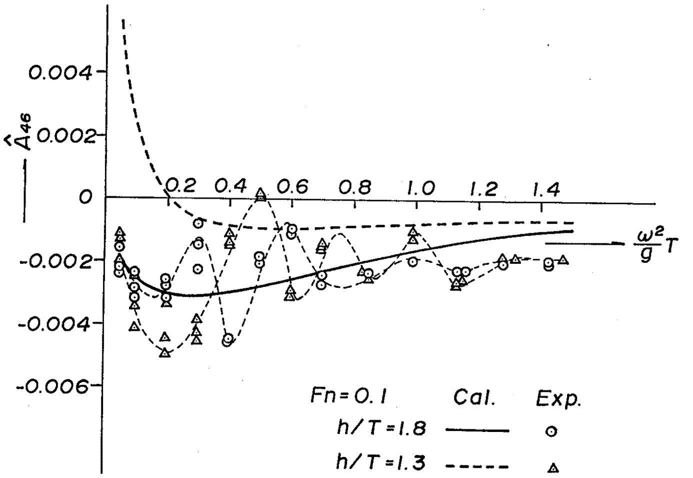

Fig. 4.37 $\hat{A}_{46}$: Coupling moment coeff. of yaw into roll at $F_n=0.10$

respectively. Similar tendency appears in the principal terms of swaying and yawing mode.

$\hat{A}_{46}$, $\hat{B}_{46}$, $\hat{A}_{64}$, $\hat{B}_{64}$

The subscript $i=4$, $j=6$ of each coefficient denotes coupling term between yawing and rolling mode. Experimental values of $\hat{A}_{46}$ and $\hat{B}_{46}$ fluctuate and show hump and hollow variations (Fig. 4.37, 4.38). Since the wave heights generated by rolling motion are smaller than ones due to yawing motion, effects of tank walls on $\hat{A}_{64}$ and $\hat{B}_{64}$ are not so strong as ones on $\hat{A}_{46}$ and $\hat{B}_{46}$ (Figs. 4.39, 4.40).

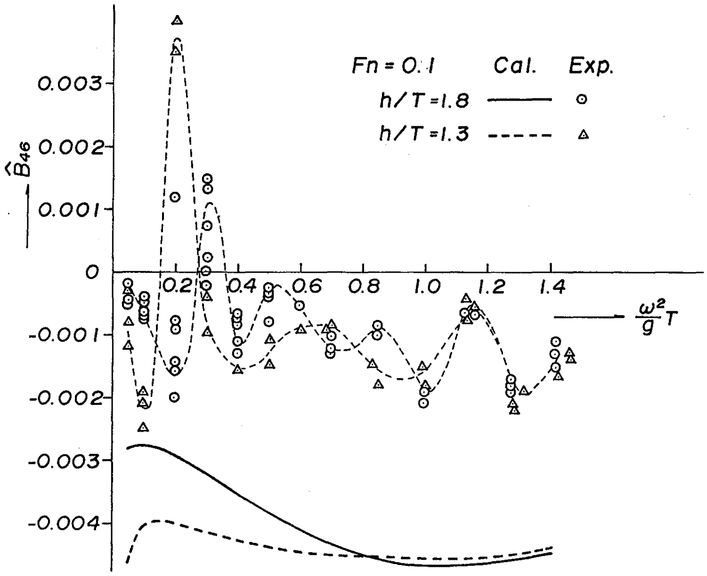

Fig. 4.38 $\hat{B}_{46}$: Coupling moment coeff. of yaw into roll at $F_n=0.10$

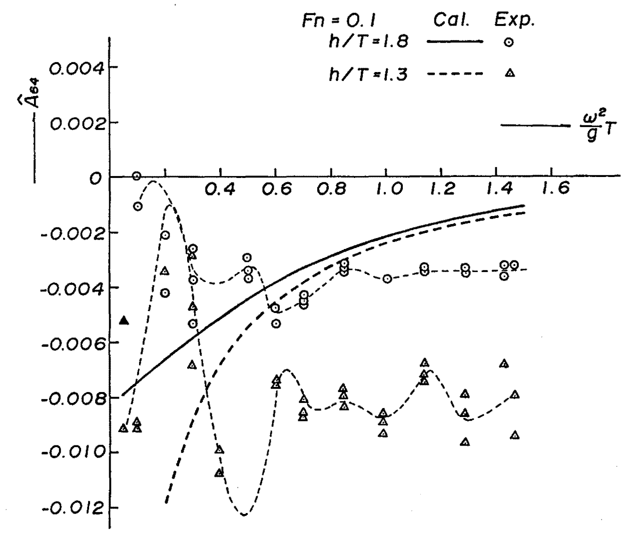

Fig. 4.39 $\hat{A}_{64}$: Coupling moment coeff. of roll into yaw at $F_n=0.10$

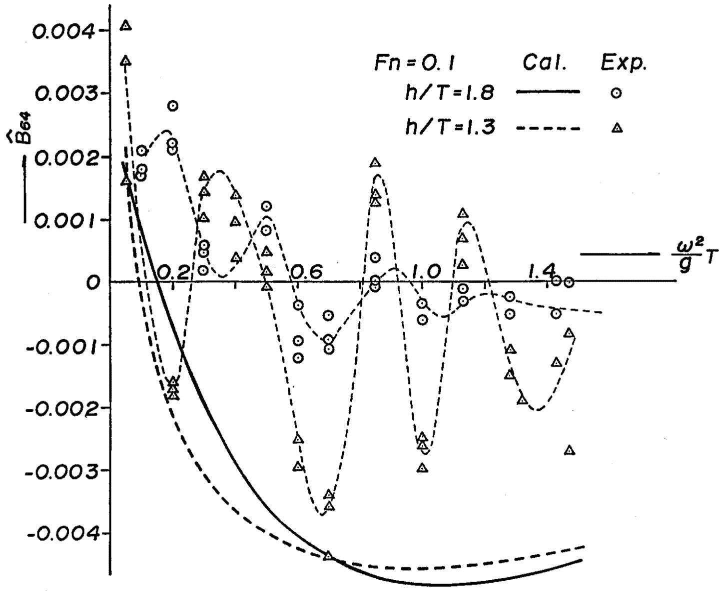

Fig. 4.40 $\hat{B}_{64}$: Coupling moment coeff. of roll into yaw at $F_n=0.10$

5. Measurement of wave exciting forces

Regular waves were generated by wave making machine installed at the end of tank and wave exciting forces and moments about the center of gravity of the ship model were measured by means of the instrument of strain gauge type. Table 2.3 shows the experimental conditions, three kinds of ship speeds, two kinds of water depths and three heading angles, for which the measurements were done. Wave exciting forces measured in beam sea condition are not shown here, because interference effects of tank walls have a little influence on these forces.

5.1 Expression of results

Non-dimensional expressions of experimental results are shown as follows:

Amplitude of force for surge : $\hat{F}_x = |F_{xe}|/\rho g\zeta_a L^2$
Amplitude of force for sway : $\hat{F}_y = |F_{ye}|/\rho g\zeta_a L^2$
Amplitude of force for heave : $\hat{F}_z = |\hat{F}_{ze}|/\rho g\zeta_a L^2$
Amplitude of moment for roll : $\hat{M}_\phi = |M_{\phi e}|/\rho g\zeta_a L^3$
Amplitude of moment for pitch : $\hat{M}_\theta = |M_{\theta e}|/\rho g\zeta_a L^3$
Amplitude of moment for yaw : $\hat{M}_\psi = |M_{\psi e}|/\rho g\zeta_a L^3$

5.2 Comparison of experimental values with theoretical ones

Wave exciting forces and moments on the ship model with various

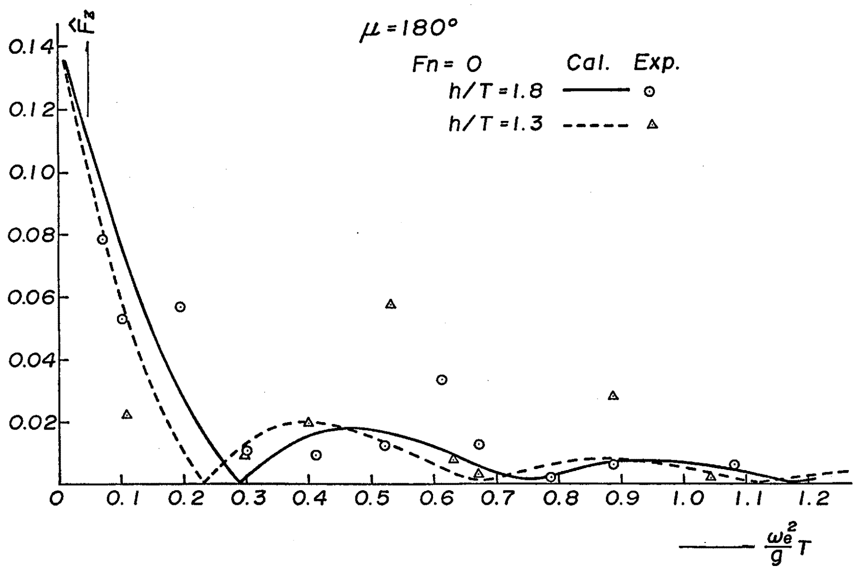

Fig. 5.1 $\hat{F}_Z$: Wave exciting forces for heave at $F_n=0$ in head sea condition

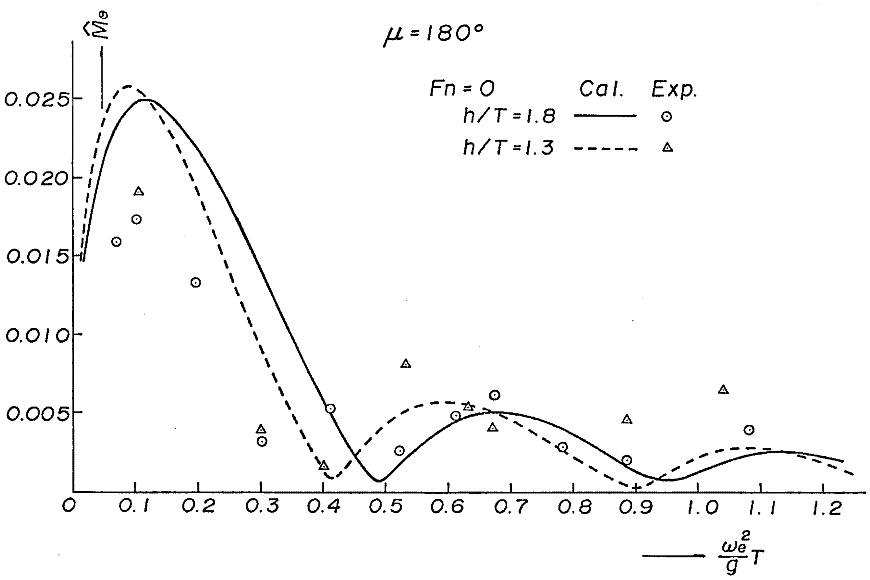

Fig. 5.2 $\hat{M}_\theta$: Wave exciting moments for pitch at $F_n=0$ in head sea condition

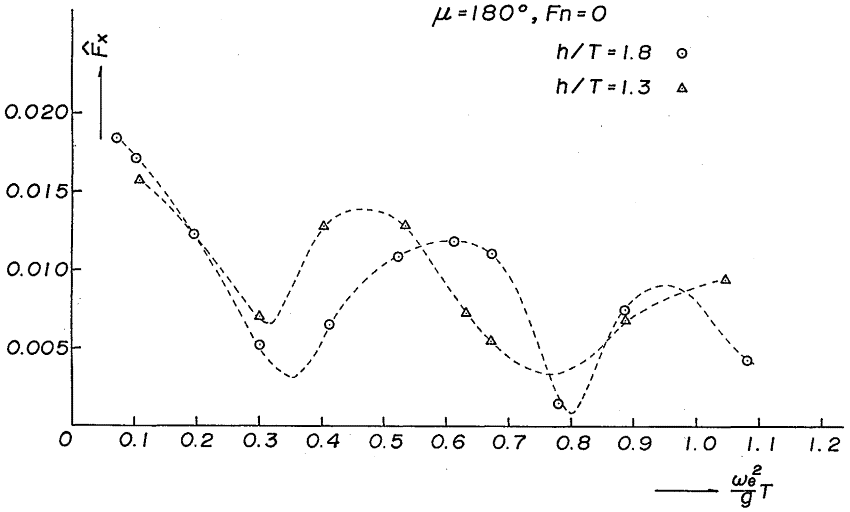

Fig. 5.3 $\hat{F}_x$: Wave exciting forces for surge at $F_n=0$ in head sea condition

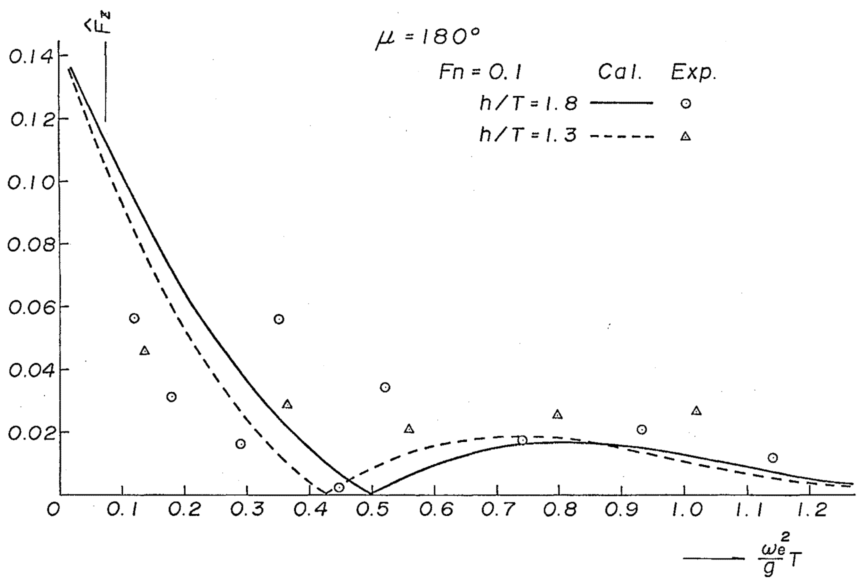

Fig. 5.4 $\hat{F}_z$: Wave exciting forces for heave at F_n=0.10 in head sea condition

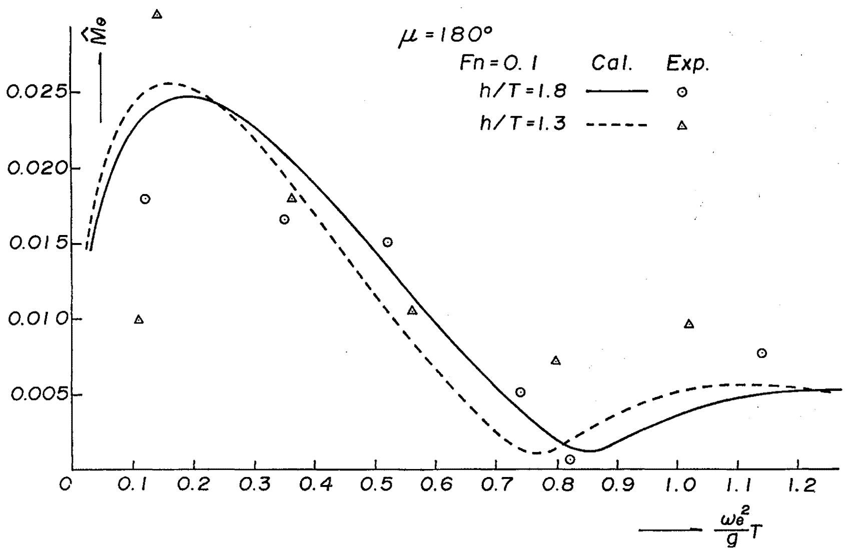

Fig. 5.5 $\hat{M}_\theta$: Wave exciting moments for pitch at F_n=0.10 in head sea condition

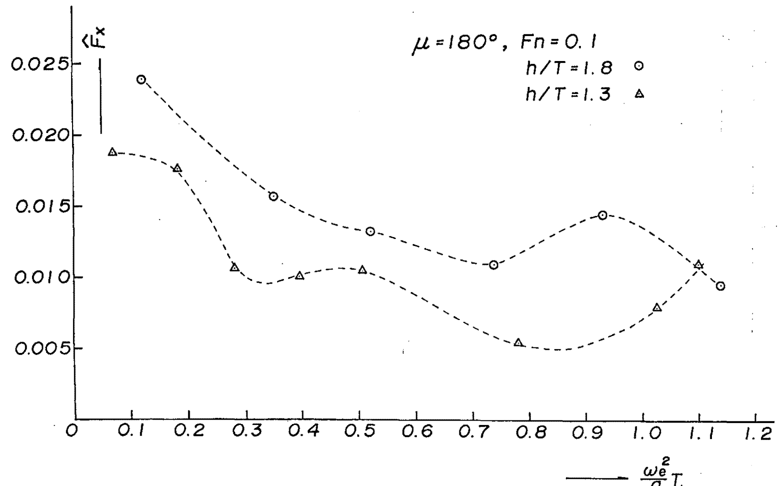

Fig. 5.6 $\hat{F}_x$: Wave exciting forces for surge at F_n=0.10 in head sea condition

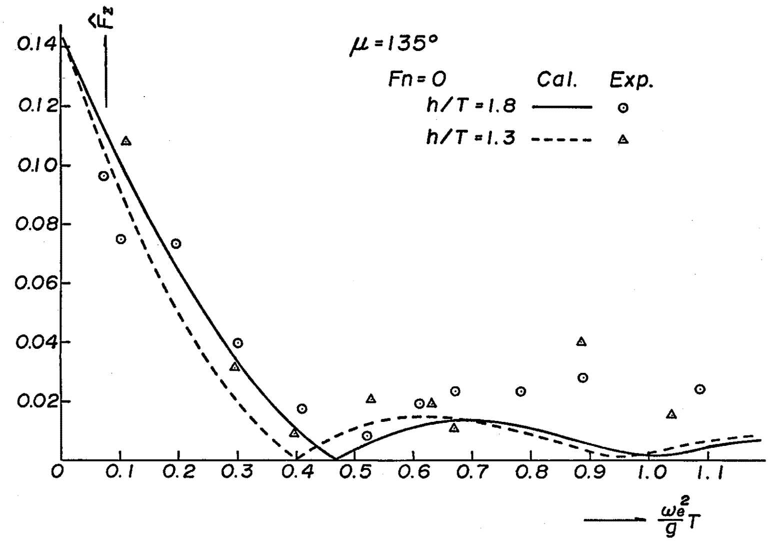

Fig. 5.7 $\hat{F}_Z$: Wave exciting forces for heave at $F_n=0$ in bow sea condition

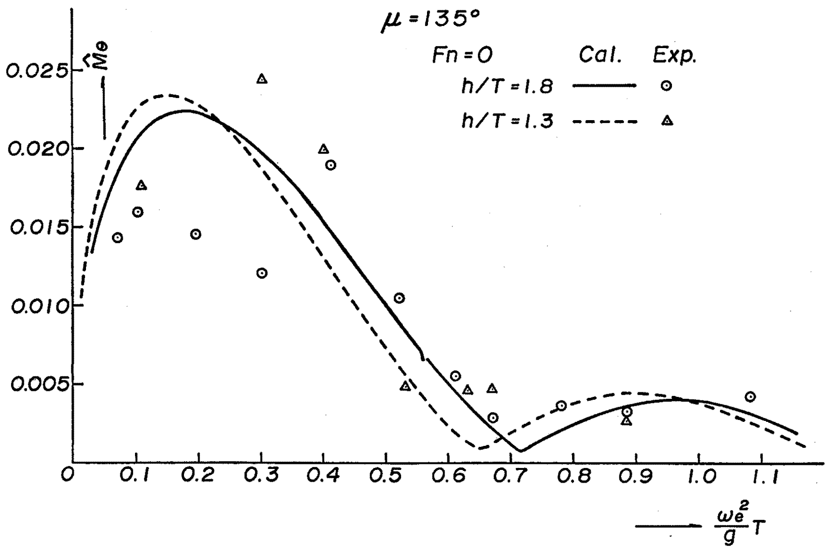

Fig. 5.8 $\hat{M}_\theta$: Wave exciting moments for pitch at $F_n=0$ in bow sea conditon

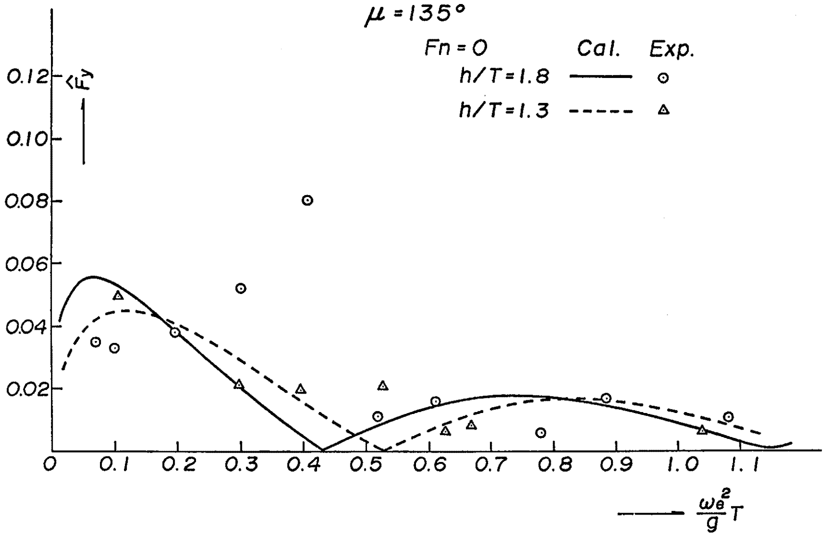

Fig. 5.9 $\hat{F}_y$: Wave exciting forces for sway at $F_n=0$ in bow sea condition

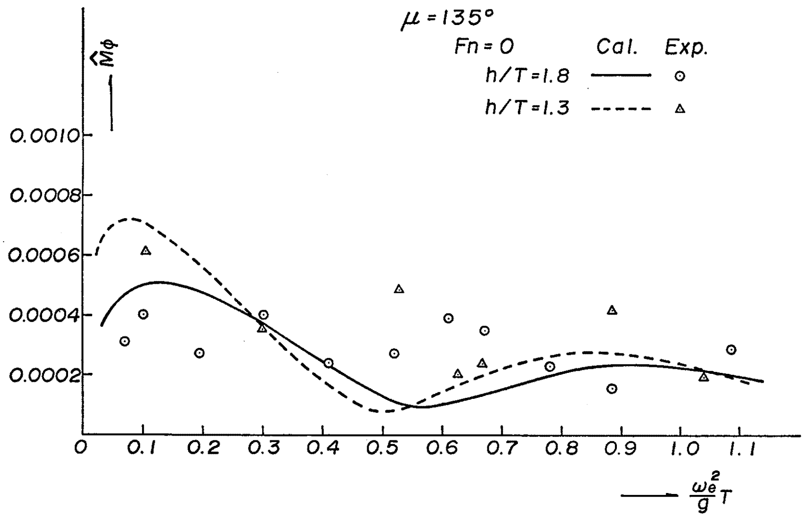

Fig. 5.10 $\hat{M}_\phi$: Wave exciting moments for roll at $F_n=0$ in bow sea condition

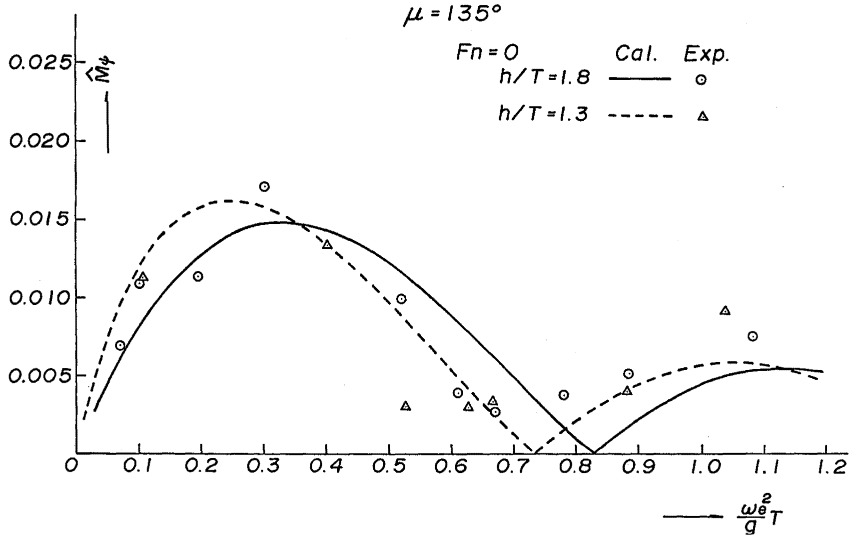

Fig. 5.11 $\hat{M}_\phi$: Wave exciting moments for yaw at $F_n=0$ in bow sea condition

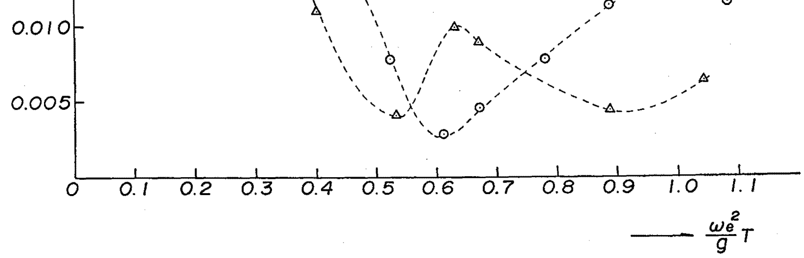

Fig. 5.12 $\hat{F}_x$: Wave exciting forces for surge at $F_n=0$ in bow sea condition

heading angles were measured in regular waves and were compared with the results of theoretical calculations obtained by new strip method described in Appendix I. These correlation works are shown in Figs. 5.1~5.12.

5.2.1 Head sea condition ($\mu=180°$)

(i) Wave exciting force for heave: $\hat{F}_z$

Experimental values are smaller than theoretical ones in low frequencies but both are in agreement in high frequencies except near the frequencies where the former ones are larger than the latter ones shown in Table 5.1 (Figs. 5.1, 5.4).

(ii) Wave exciting moment for pitch: $\hat{M}_\theta$

Theoretical values of pitching moment $\hat{M}_\theta$ have a maximum peak in the region of low frequencies and its maximum value becomes larger as the depth of water becomes more shallow. Experimental values of $\hat{M}_\theta$ are smaller than theoretical ones in low frequencies, while in high frequencies experimental values are in agreement with theoretical ones except near the frequencies where the former ones show humps as shown in Table 5.1 (Fig. 5.2, 5.5).

(iii) Wave exciting force for surge: $\hat{F}_x$

Although experimental values of wave exciting surging forces $\hat{F}_x$ show scattering, these values increase as a frequency $\left(\frac{\omega_e^2}{g}T\right)$ changes from high frequency to low frequency. Effects of tank walls do not appear clearly in experimental results.

From the above results in (i), (ii) and (iii), it is seen that effects of tank walls on wave exciting forces and moments are not so strong as on the radiation forces obtained by forced oscillating tests in spite of the ship model position parallel to the tank wall.

Table 5.1 Frequencies $\left(\frac{\omega_e^2}{g}T\right)$ when the max. values of $\hat{F}_Z$ and $\hat{M}_\theta$ appear in head sea condition

	ship speed	$h/T=1.3$	$h/T=1.8$
		$\frac{\omega_e^2}{g}T$	$\frac{\omega_e^2}{g}T$
$\hat{F}_z$	$F_n=0$	0.5, 0.9	0.6
	$F_n=0.075$	0.5, 0.9	0.3, 0.65, 1.0
	$F_n=0.10$	0.5, 1.0	0.35, 0.65
$\hat{M}_\theta$	$F_n=0$	0.5, 0.9, 1.05	—
	$F_n=0.075$	—	—
	$F_n=0.10$	1.0	—

5.2.2 Bow sea condition ($\mu=135°$)

Experimental values of wave exciting forces and moments for heaving, pitching, swaying, rolling and yawing mode generally agree with results of theoretical calculations except at some frequencies $\left(\frac{\omega_e^2}{g}T\right)$ shown in Table 5.2 where experimental values are larger than theoretical ones, because of interference effects of tank walls.

Table 5.2 Frequencies $\left(\frac{\omega_e^2}{g}T\right)$ when the max. values of wave exciting forces and moments appear at $F_n=0$ in bow sea condition

	$h/T=1.3$	$h/T=1.8$
	$\frac{\omega_e^2}{g}T$	$\frac{\omega_e^2}{g}T$
$\hat{F}_Z$	0.5, 0.9	0.2, 0.7, 0.9
$\hat{M}_\theta$	0.3, 0.7, 0.9	0.4
$\hat{F}_y$	0.4, 0.5	0.4, 0.8
$\hat{M}_\phi$	0.5, 0.9	0.2, 0.6~0.7, 0.9
$\hat{M}_\psi$	0.3, 0.5, 1.05	0.3, 0.8~0.9

6. Ship motions in regular waves

We measured amplitudes of motions of the ship model by means of an apparatus measuring motions of 6-degrees of freedom. Measurements of motions of the ship model were carried out at three heading angles which were 180 degrees (head sea condition), 135 degrees (bow sea condition) and 90 degrees (beam sea condition). Since it is seen that interference effects of tank walls scarcely affect amplitudes of motions in beam sea condition, the results in this condition are not shown in this paper.

6.1 Comparison of measured amplitude with computed one

(i) Head sea condition ($\mu=180°$)

Heaving and pitching amplitudes become smaller in low frequencies for both experiments and theoretical predictions as the depth of water becomes more shallow. Experimental values are in good agreement with theoretical ones except near frequencies shown in Table 6.1, where experimental amplitudes of ship motions are larger than computed ones by new strip method. These frequencies at which humps of response curves of ship motions appear are independent of ship speed. Such phenomena appear more stronger in heaving response curves than in pitching response curves (Figs. 6.1, 6.2, 6.4, 6.5).

Effects of tank walls do not appear clearly in surging response curves (Figs. 6.3, 6.6).

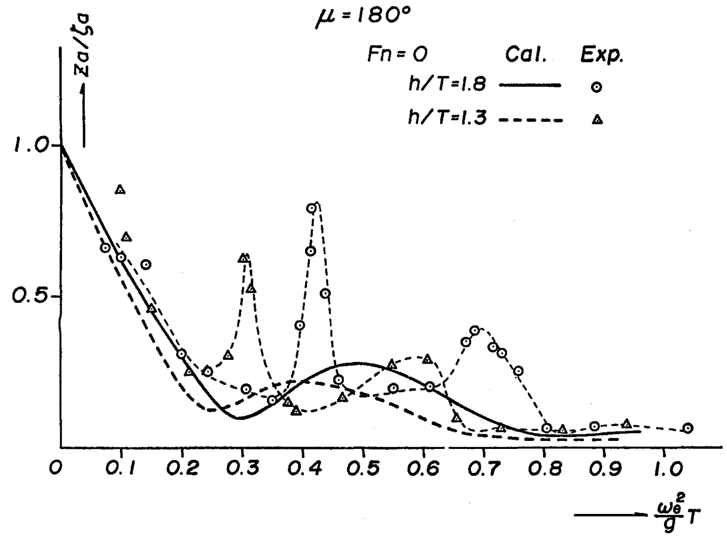

Fig. 6.1 Heaving amplitudes at $F_n=0$ in head sea condition

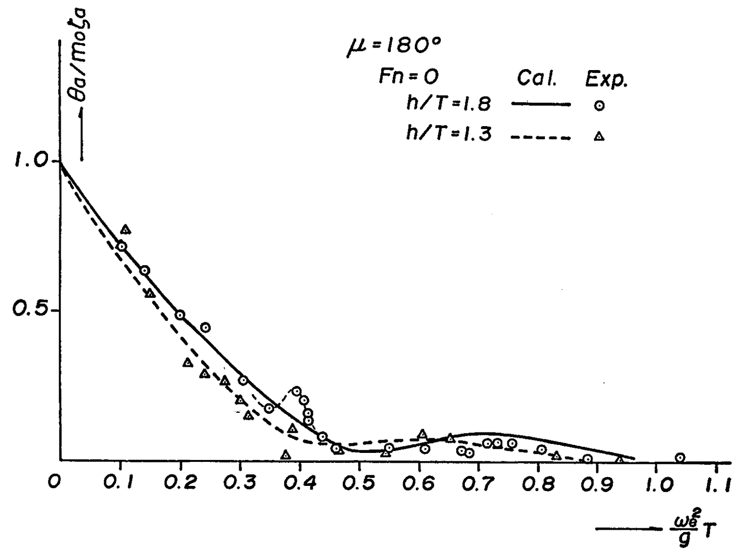

Fig. 6.2 Pitching amplitudes at $F_n=0$ in head sea condition

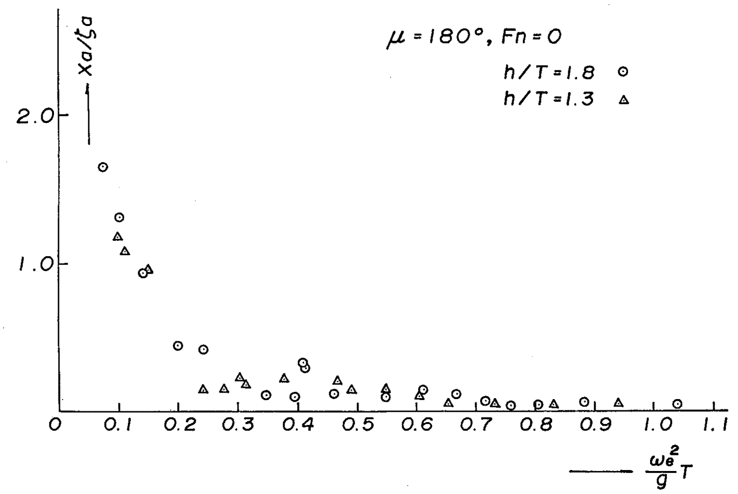

Fig. 6.3 Surging amplitudes at $F_n=0$ in head sea condition

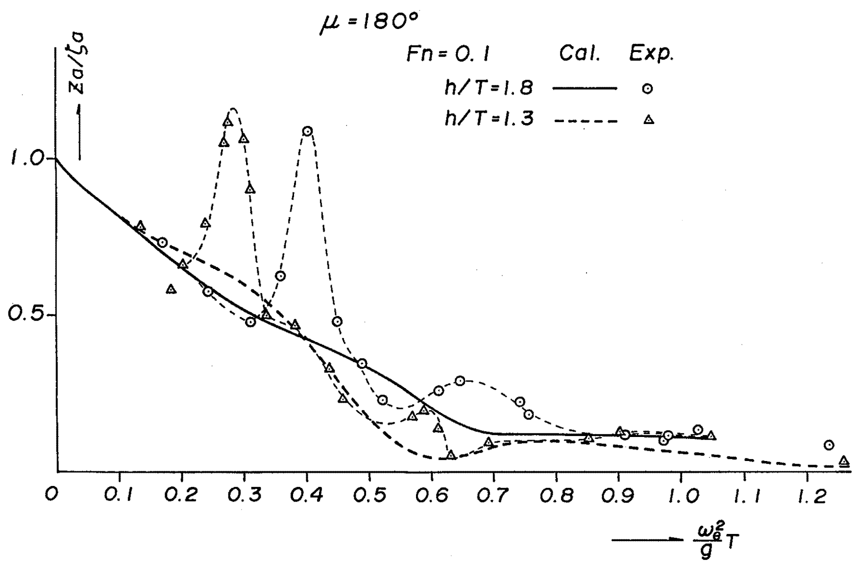

Fig. 6.4 Heaving amplitudes at $F_n=0.10$ in head sea condition

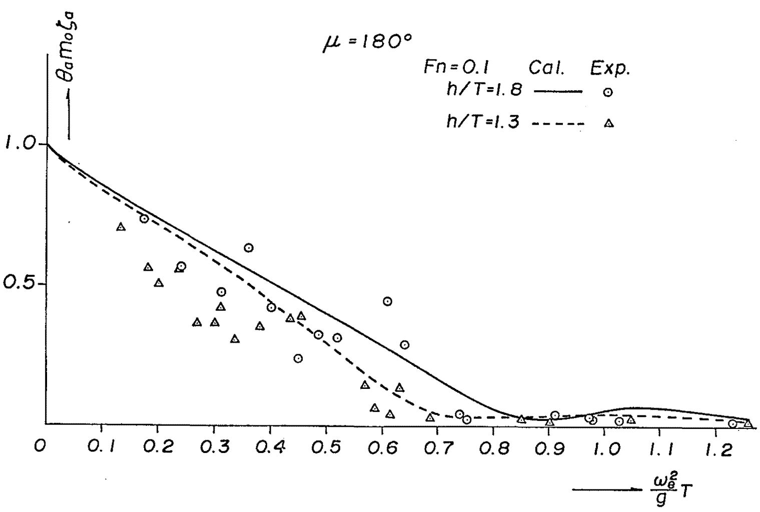

Fig. 6.5 Pitching amplitudes at $F_n=0.10$ in head sea condition

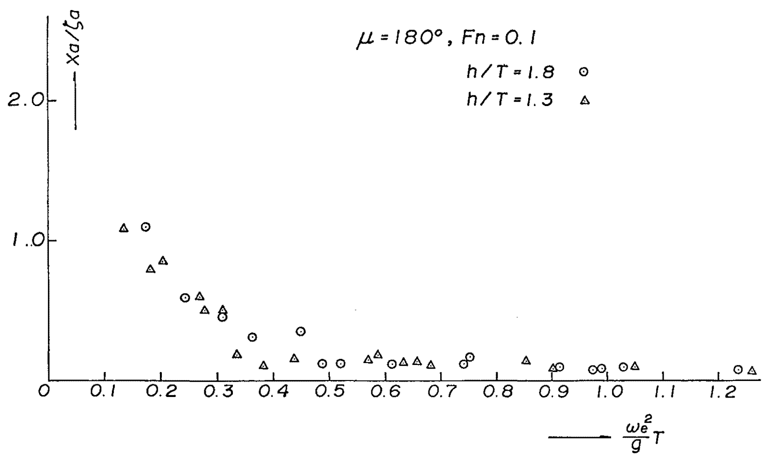

Fig. 6.6 Surging amplitudes at $F_n=0.10$ in head sea condition

(ii) Bow sea condition ($\mu=135°$)

Experimetal amplitudes of ship motions in bow sea condition are in agreement with those obtained with theoretical computations except near frequencies shown in Table 6.2, where the formers are larger than the latters. The phenomena of sharp humps in response curves of ship motions appear strongly in longitudinal motions rather than in lateral motions, and especially appear strongly in heaving response curves.

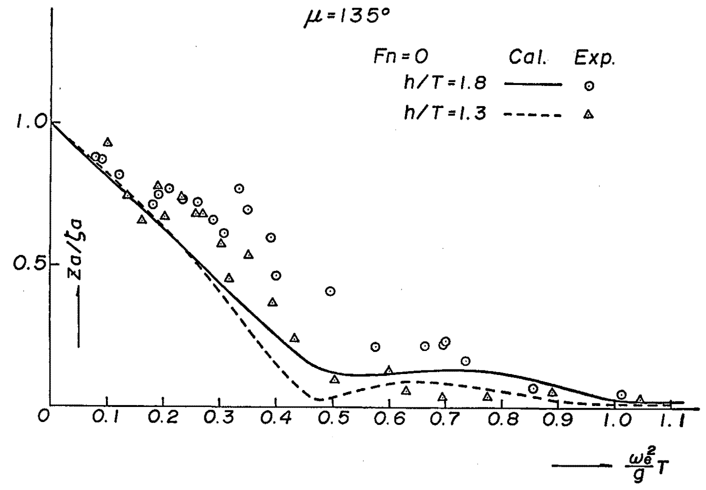

Fig. 6.7 Heaving amplitudes at $F_n=0$ in bow sea condition

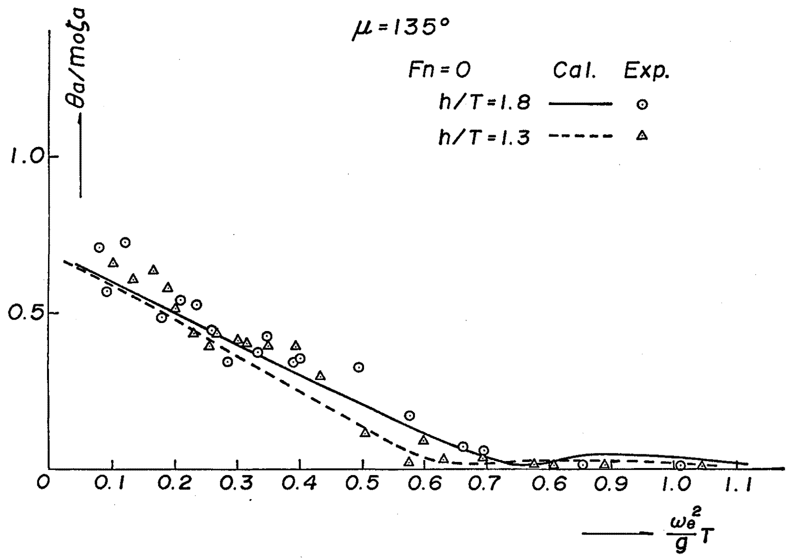

Fig. 6.8 Pitching amplitudes at $F_n=0$ in bow sea condition

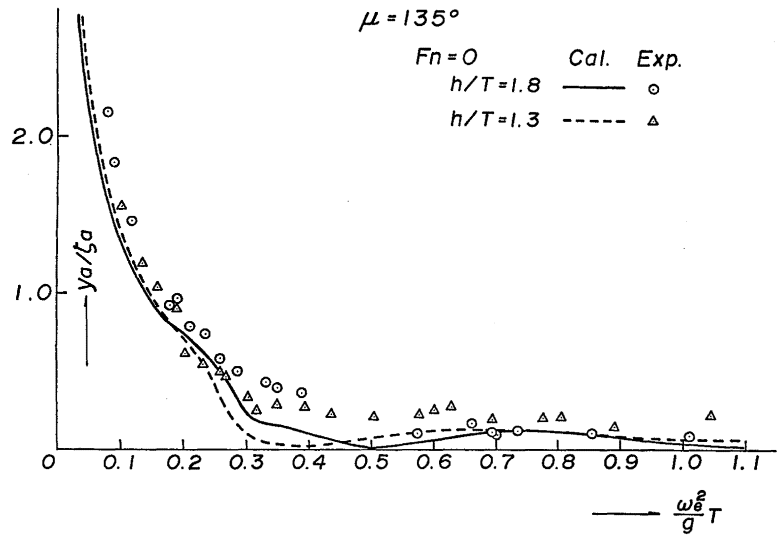

Fig. 6.9 Swaying amplitudes at $F_n=0$ in bow sea condition

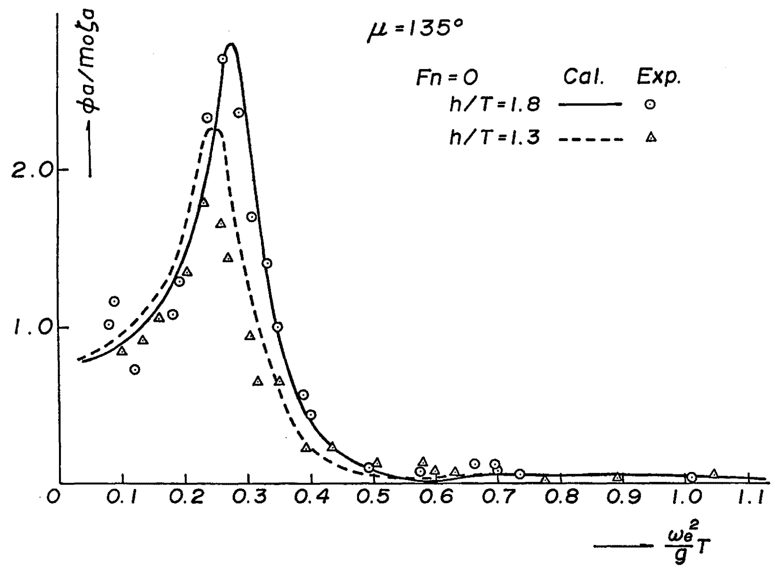

Fig. 6.10 Rolling amplitudes at $F_n=0$ in bow sea condition

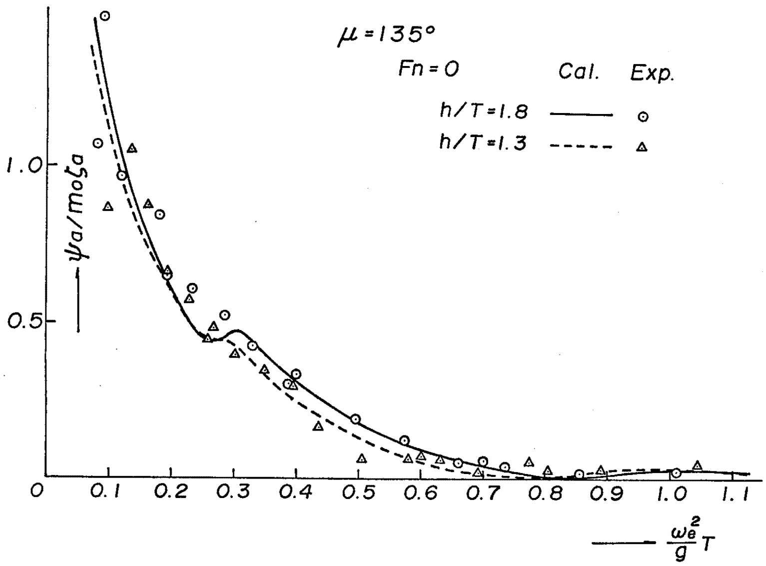

Fig. 6.11 Yawing amplitudes at $F_n=0$ in bow sea condition

Table 6.1 Frequencies $\left(\frac{\omega_e^2}{g}T\right)$ when humps of response curves appear in head sea condition

		$h/T=1.3$ $\frac{\omega_e^2}{g}T$	$h/T=1.8$ $\frac{\omega_e^2}{g}T$
Heave (Z_a/ζ_a)	$F_n=0$	0.3, 0.6	0.4, 0.7
	$F_n=0.075$	0.3, 0.55	0.4, 0.7
	$F_n=0.10$	0.3, 0.6	0.4, 0.7
Pitch ($\theta_a/m_0\zeta_a$)	$F_n=0$	0.3	0.4
	$F_n=0.075$	0.3	0.4
	$F_n=0.10$	0.3	0.6

Table 6.2 Frequencies $\left(\frac{\omega_e^2}{g}T\right)$ when humps of response curves appear in bow sea condition

	$h/T=1.3$ $\frac{\omega_e^2}{g}T$	$h/T=1.8$ $\frac{\omega_e^2}{g}T$
Heave	0.25	0.35, 0.50
Pitch	0.4	0.5
Sway	——	——
Roll	——	——
Yaw	——	——

6.2 Effects of interference of tank walls

From the results shown in previous section it is seen that theoretical response curves derived by new strip theory generally agree with the mean curves of these experimental response after smoothing the hump and hollow variations obtained in experiments. These humps and hollows are thought to be induced by the interference of tank walls and heuristic explanation of the mechanism of this phenomenon will be given hereafter.

6.2.1 Critical circular frequency of wall effect in motions of a ship

Wave pattern which are generated by a periodic source point running with a constant forward speed in water of finite depth can be given by the following equations. [6,13]

$$
\left\{
\begin{array}{ll}
|y|/x=-\dfrac{\tan\theta_{A1n}}{\tan^2\theta_{A1n}+\sec^2\theta_{A1n}\sqrt{1+4\Omega\cos\theta_{A1n}/\tanh n_1h}} & : A_1\text{-Wave,} \\
\qquad 0<\theta_{A1n}<\dfrac{\pi}{2} & \\
|y|/x=\dfrac{\tan\theta_{A2n}}{\tan^2\theta_{A2n}-\sec^2\theta_{A2n}\sqrt{1+4\Omega\cos\theta_{A2n}/\tanh n_1h}} & : A_2\text{-Wave,} \\
\qquad 0<\theta_{A2n}<\dfrac{\pi}{2} & \\
\left.\begin{array}{l}
|y|/x=-\dfrac{\tan\theta_{B1n}}{\tan^2\theta_{B1n}+\sec^2\theta_{B1n}\sqrt{1-4\Omega\cos\theta_{B1n}/\tanh n_2h}} : B_1\text{-Wave} \\
|y|/x=-\dfrac{\tan\theta_{B2n}}{\tan^2\theta_{B2n}-\sec^2\theta_{B2n}\sqrt{1-4\Omega\cos\theta_{B2n}/\tanh n_2h}} : B_2\text{-Wave}
\end{array}\right\} & \\
\qquad \Omega<\dfrac{\tanh n_2h}{4}:\ 0<\theta_{B1n},\ \theta_{B2n}<\dfrac{\pi}{2}, & \\
\qquad \Omega>\dfrac{\tanh n_2h}{4}:\ \cos^{-1}\dfrac{1}{4\Omega}<\theta_{B1n},\ \theta_{B1n}<\dfrac{\pi}{2}. &
\end{array}
\right.
\qquad \cdots\cdots\cdots (6.1)
$$

where

$\Omega=\dfrac{\omega V}{g}$

ω : circular frequency of wave

V : ship speed

$\left.\begin{array}{l}n_1\\n_2\end{array}\right\}$: real root of equation: $\left(\dfrac{\omega}{V}\pm m\right)^2-\dfrac{g}{V^2}n\tanh nh=0$

When a ship is making small motions with a frequency ω and a forward speed V in a canal, an angle β between a center line of a ship and a direction of propagating wave generated by a bow of a ship is represented by a maximum value of $\tan^{-1}|y|/x$ obtained due to (6.1). Let β_c denote the critical angle[5] between her center line and the direction of propagating wave, when a wave generated by a bow of a ship is reflected by tank wall and the reflected wave encounters a stern of a ship again. Then there exists the following relationship among these values (β_c, L_{pp}, B_w).

$$L_{pp}\cdot\tan\beta_c = B_w \qquad \cdots\cdots\cdots\cdots (6.2)$$

where L_{pp} : Length of ship model (=3 m)
B_w : Breadth of canal (=4 m)

The critical angle β_c in our experiment is

$$\beta_c = \tan^{-1}(4/3) = 53.1 \text{ (degrees)}.$$

The critical circular frequency ω_c in the conditions of this experiment is estimated from curves shown in Fig. 6.12 as follows:

$$\Omega = 0.428$$

$$Fn = 0.10 : \omega_c = 7.735, \quad \frac{\omega_c^2}{g} T = 1.186$$

$$Fn = 0.075 : \omega_c = 10.314, \quad \frac{\omega_c^2}{g} T = 2.105 \qquad \cdots\cdots\cdots\cdots (6.3)$$

It is seen from Fig. 6.12 angle β is mostly independent of water depth in this experiment. Circular frequencies in this experiment are smaller than the critical circular frequencies ω_c given in equation (6.3). Consequently results obtained in this experiment are clearly affected by interference effects of

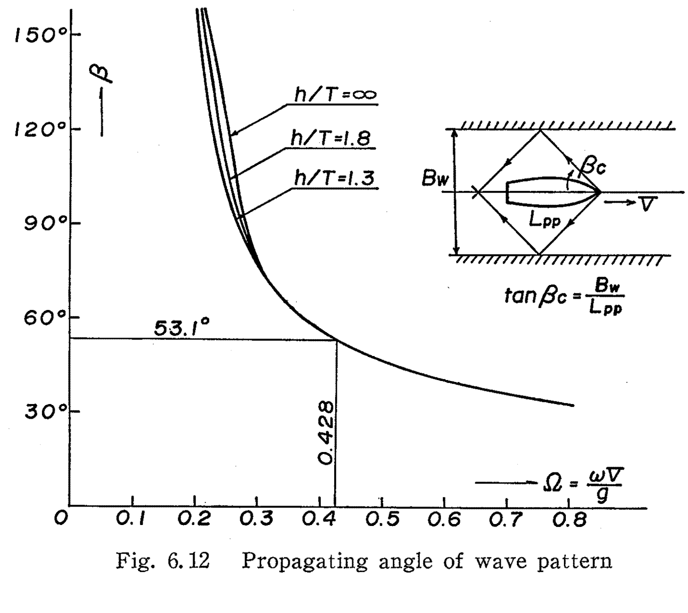

Fig. 6.12 Propagating angle of wave pattern

tank walls at overall frequencies.

6.2.2 Two dimensional standing wave and hydrodynamic forces on a ship model in a canal

Putting a wave number without a forward speed as m_0, the following equation is obtained from (6.1).

$$\frac{\omega^2}{g} = m_0 \tanh m_0 h \qquad \cdots\cdots\cdots\cdots (6.4)$$

The relationships between wave numbers and oscillating frequencies in this experiment are shown in Fig. 6.13.

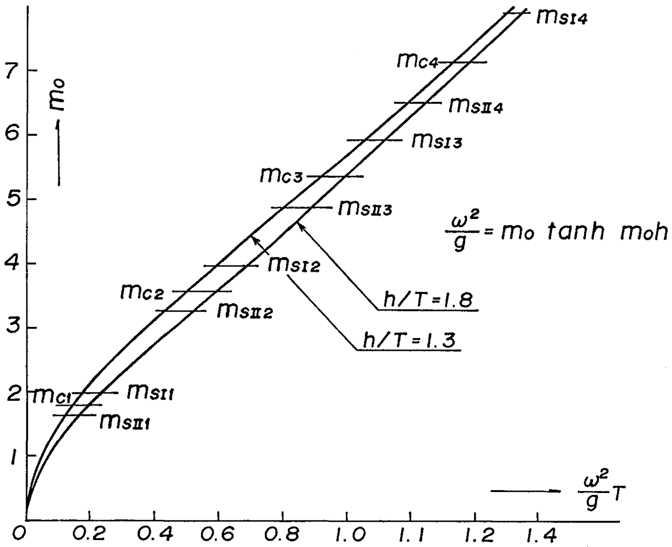

Fig. 6.13 Relation between oscillating frequency and wave number of two dimensional standing wave

(i) Symmetric motion

When a infinitely long ship is forced to make heaving oscillation at the center of a canal, it is supposed that two-dimensional standing waves are generated on the water surface between a ship model and tank walls at frequencies whose wave numbers are given by following equation:

$$m_{ck} = \frac{\pi}{(B_w - B)/2} k = 1.792k, \quad (k=1, 2, 3 \cdots) \qquad \cdots\cdots\cdots\cdots (6.5)$$

where B_w : Breadth of canal (=4 m)
B : Breadth of ship model (=0.493 m)

Non-dimensional frequencies $\left(\frac{\omega^2}{g} T\right)$ of two-dimensional standing waves with wave numbers given by (6.5) are obtained according to Fig. 6.13 and are shown in Table 6.1.

Heaving damping coefficients $\hat{B}_{33}$ obtained by forced heaving tests are larger than theoretical values without considering effects of tank walls at the frequencies shown in Table 6.3 and these frequencies are nearly equal to ones at which heaving damping coefficient $\hat{B}_{33}$ reach maximum value (Table 4.2).

Standing waves with high amplitude will be generated on the water surface between the ship body and tank wall at wave number m_{ck} and these waves will diffuse much energy because they propagate to the longitudinal directions of the canal. On the contrary, damping coefficients of heaving $\hat{B}_{33}$ by forced heaving test take the minimum values (Table 4.2) much smaller than theoretical values at nearly middle frequency between neighbouring two frequencies shown in Table 6.1.

Wave exciting forces of heaving also become larger at the same frequencies as the damping coefficients of heaving $\hat{B}_{33}$ become larger (Table 4.2, 5.1)

We cannot give such a simple explanation on the causes of humps and hollows appearing in hydrodynamic moments of pitching as we could do in heaving forces, because three-dimensional effects may be stronger in pitching moment.

Table 6.3 Frequencies $\left(\frac{\omega^2}{g}T\right)$ when two-dimensional standing waves are generated in the canal

		$h/T=1.3$	$h/T=1.8$
		$\frac{\omega^2}{g}T$	$\frac{\omega^2}{g}T$
Wave number	$m_{c1}=1.792$	0.145	0.192
	$m_{c2}=3.584$	0.50	0.59
	$m_{c3}=5.376$	0.912	0.994
	$m_{c4}=7.168$	1.325	1.379

(ii) Asymmetric motion

Forced swaying tests were carried out by shifting the ship model 0.17 m to the side of the tank from the center line so that the her center line was parallel to the tank wall. Suppose that a infinitely long ship is forced to make swaying oscillation away 0.17 m to the side of the tank from center line, two different wave numbers exist for two-dimensional standing waves generated on water surface between the ship body and tank walls, and they are given as follows:

$$m_{s\,\mathrm{I}\,k}=\frac{\pi}{(B_w-B)/2-0.17}k=1.984\,k, \quad (k=1,2,3\cdots) \qquad \cdots\cdots\cdots (6.6)$$

$$m_{s\,\mathrm{II}\,k}=\frac{\pi}{(B_w-B)/2+0.17}k=1.633\,k, \quad (k=1,2,3\cdots) \qquad \cdots\cdots\cdots (6.7)$$

When two-dimensional standing wave with the wave number of either (6.6) or (6.7) is generated on water surface between the ship body and tank walls, the hydrodynamic forces of swaying mode will become larger. Non-dimensional frequencies $\left(\frac{\omega^2}{g}T\right)$ of standing waves with the wave numbers given by (6.6) and (6.7) are obtained from Fig. 6.12 and are shown in Table 6.4.

From above table and Fig. 4.22 it is seen that the damping coefficients of swaying $\hat{B}_{22}$ reach the maximum value and larger than those obtained by new strip theory without considering effects of tank wall near the frequencies at which two-dimensional standing waves are generated in the narrow water way between the ship body and tank wall, that corresponds to (6.6). On the contrary, it is seen that damping coefficients of swaying $\hat{B}_{22}$ take the minimum value near the middle frequency between neighbouring two frequencies shown in Table 6.2 ($\hat{B}_{22}$ in Table 4.3).

Because of strong three-dimensional effects on hydrodynamic moments of yawing mode, it is difficult to explain the causes of hump and hollow variations in yawing moments with considering only two-dimensional standing waves ($\hat{B}_{66}$ in Table 4.5).

Table 6.4 Frequencies $\left(\frac{\omega^2}{g}T\right)$ when two-dimensional standing waves are generated in the canal

		$h/T=1.3$	$h/T=1.8$
		$\frac{\omega^2}{g}T$	$\frac{\omega^2}{g}T$
Wave numbers of Eq. (6.6)	$m_{sI_1}=1.984$	0.178	0.230
	$m_{sI_2}=3.968$	0.585	0.678
	$m_{sI_3}=5.952$	1.045	1.115
Wave numbers of Eq. (6.7)	$m_{sII1}=1.633$	0.120	0.165
	$m_{sII2}=3.266$	0.430	0.514
	$m_{sII3}=4.899$	0.795	0.882
	$m_{sII4}=6.532$	1.180	1.240

6.2.3 Natural period of heaving oscillation and amplitudes of ship motions

Heaving response curves also are mostly affected by interference effects of tank walls due to reflection from wall sides of tank in regular waves. As shown in Fig. 4.1 and Fig. 4.2 heaving added mass coefficients of the ship in the canal show hump and hollow variations due to effects of tank walls. With taking effects of tank wall into account natural periods of heaving oscillation of ship in the canal have been evaluated as follows: neglecting the coupling effect of pitching motion in (3.2), we get following equation.

$$\omega^2 = \rho g A_w / (M + A_{33})$$

$$M + A_{33} = \frac{\rho g A_w}{\frac{\omega^2}{g} T} \cdot \frac{T}{g}$$

$$\therefore \hat{M} + \hat{A}_{33} = (M + A_{33}) / \rho L^3 = \frac{A_w \cdot T}{\xi_d \cdot L^3} \qquad \cdots\cdots\cdots\cdots (6.8)$$

where A_w : Water plane area of ship
L : Length of ship

A natural circular frequency of heaving oscillation can be evaluated from the frequency at a cross point where the curve obtained by (6.8) intersects the curves of virtual mass coefficients $(\hat{M}+\hat{A}_{33})$ obtained by forced oscillating tests. From the graphs shown in Figs. 4.1, 4.2 it is seen that there can be two natural circular frequencies in this experiment. Natural frequencies $\left(\frac{\omega^2}{g} T\right)$ of heaving oscillation estimated from these figures are shown in Table 6.5.

Table 6.5 Natural frequencies $\left(\frac{\omega^2}{g} T\right)$ of heaving

		$h/T=1.3$	$h/T=1.8$
		$\frac{\omega^2}{g} T$	$\frac{\omega^2}{g} T$
Ship speed	$F_n=0$	0.31, 0.61	0.41, 0.75
	$F_n=0.075$	0.30, 0.55	0.43, 0.6~0.65
	$F_n=0.10$	0.30, 0.55	0.40, 0.6~0.65

It is seen from Fig. 6.1 and Fig. 6.4 that experimental values of heaving amplitudes rapidly increase near these natural frequencies of heaving oscillation. The natural frequencies shown in Table 6.5 coincide with frequencies at which damping coefficients $\hat{B}_{33}$ of heaving mode have the minimum value (Table 4.2).

Heaving amplitudes of the ship model in our experiment are very large, since the amplitude of ship motion is generally very large when the damping coefficient is small at the response frequency of that motion of a ship.

7. Conclusion

The main conclusions obtained from this investigation are summarized as follows.

(1) When the ship model is set in the tank so that her center line is perpendicular to the tank wall, radiation forces and wave exciting forces acting on the ship model in the canal are scarcely affected by interference effects

of tank walls. Consequently amplitudes of motions in regular waves can be estimated by the strip theory without considering effects of tank walls.

(2) When the ship model is set in the tank so that her center line is parallel to the tank wall, hydrodynamic forces acting on the ship model show hump and hollow variations which depend on oscillating frequencies. The response curves of motions in regular waves show the similar phenomena to the hydrodynamic forces. These hump and hollow variations are considered to be interference effects of tank walls and cannot be estimated by usual strip theory in which effects of tank walls are not taken into account.

(3) The frequencies, at which hump and hollow variations appear in hydrodynamic forces due to effects of tank walls mentioned in (2), can be estimated by assuming a simple model in which two-dimensional standing waves are generated in water surface between the ship body and tank walls.

(4) Effects of tank walls affecting the amplitudes of pitching oscillation in head sea condition are smaller than ones of heaving oscillation on comparing these response curves. In the bow sea condition (where center line of ship is set at an angle of 45 degrees to the tank wall) hump and hollow variations of heaving response curve do not appear so strongly as those in head sea condition. Hump and hollow variations due to effects of tank walls scarcely appear in the response curves of swaying, rolling and yawing motions in bow sea condition.

Acknowledgement

The authors are grateful to Professor T. Suhara and Research Associate H. Hiyama of Kyushu University for their useful suggestions and valuable discussions in designing the canal in this study. And they also wish to express their thanks to Research Associate H. Arakawa, Engineers Mr. M. Yasunaga and Mr. M. Inada for their coorporations in experiments and are indebted to Miss. M. Hojo and Miss. H. Yokobayashi for their generous assistances in preparing the manuscripts.

This study was based on the grant in aid for scientific research of the Ministry of Education: Scientific Research (B) (Title of project: Seakeeping Qualities of the Ship in Shallow Water, Project number 146101).

The calculations of hydrodynamic forces and ship motions were performed by means of the FACOM 230-75 of the Computer Center of Kyushu University and the FACOM 230-48 of the Computer Room of Research Institute for Applied Mechanics in Kyushu University.

References

1) Hanaoka, T., On the Side-Wall Effects on the Ship Motions among Waves in a Canal, J. S. N. A. of Japan, Vol. 102, 1958.
2) Hosoda, R., Side Wall Effects of Towing Tank on the Results of Experiments in Waves (1), J. S. N. A. of Japan, Vol. 139, 1976.

3) Vossers & Swaan, Some Seakeeping Tests with a Victory Model, I. S. P., No. 69, 1960.
4) Murdy, D. C., Some effect of Tank Wall Influence on the Results of Experiments in Waves, 13th I. T. T. C. Report of Seakeeping Committee Appendix II, 1972.
5) Takezawa, S. & Jingu, N., Testing Ship Models on Longitudinal Ship Motions by Transient Response Method (Part 5, Side Wall Effect), J. S. N. A. of Japan, Vol. 136, 1974.
6) Hanaoka, T., On the Velocity potential in Michell's System and the Configuration of the Wave Ridges due to a Moving Ship, J. S. N. A. of Japan, Vol. 93, 1952.
7) Isshiki, H., Water Waves in a Long Canal—The Velocity Potential of Periodic Source—, J. S. N. A. of Japan, Vol. 137, 1975.
8) Ohkusu, M., The Analysis of Wave Forces Acting upon Mult-Float Supported Platforms, Transactions of the West-Japan Society of Naval Architects, No. 51, 1976.
9) Takaki, MI., On the Ship Motions in Shallow Water (Part 3)—Comparison of the Experimental Results with the Calculated Results of Ship Motions in Waves—, Transactions of the West-Japan Society of Naval Architects, No. 54, 1977.
10) Takaki, MI., On the Ship Motions in Shallow Water (Part 1), Transactions of the West-Japan Society of Naval Architects, No. 50, 1975.
11) Takaki, MI., On the Ship Motions in Shallow Water (Part2)—Two Dimensional Hydrodynamic Coefficients for Swaying and Rolling Cylinder in Shallow Water—, Transactions of the West-Japan Society of Naval Architects, No. 52, 1976.
12) Takaki, MI. & Tasai, F., On the Hydrodynamic Derivative Coefficients of the Equations for Lateral Motions of Ships, Transactions of the West-Japan Society of Naval Architects, No. 46, 1973.
13) Takagi, M. & Ganno, M., A Calculation of Finite Depth Effect on Ship Motions in Waves, J. S. N. A. of Japan, Vol. 122, 1967.

(Received April 24, 1978)

Appendix I

The hydrodynamic coefficients of equations (3. 2) and (3. 3) can be obtained by new strip method without considering effects of tank walls as follows.

The coefficients for longitudinal motions:

$$\left[\begin{array}{lll} A_{33}=\int_L M_H dx_b, & B_{33}=\int_L N_H dx_b, & C_{33}=\rho g A_w, \\ A_{35}=\int_L M_H\cdot x_b dx_b, & B_{35}=\int_L (N_H\cdot x_b - VM_H) dx_b, & C_{35}=\int_L (\rho g B_x\cdot x_b - VN_H) dx_b, \end{array}\right. \qquad \cdots\cdots\cdots\cdots(\mathrm{A}\cdot 1)$$

$$\left[\begin{array}{lll} A_{55}=\int_L M_H x_b^2 dx_b, & B_{55}=\int_L \left\{N_H x_b^2+\left(\frac{V}{\omega_e}\right)^2 N_H\right\} dx_b, & C_{55}=\int_L (\rho g B_x\cdot x_b^2 - V^2 M_H) dx_b, \\ A_{53}=A_{35}, & B_{53}=\int_L \{N_H\cdot x_b + VM_H\} dx_b, & C_{53}=\int_L (\rho g B_x\cdot x_b + VN_H) dx_b. \end{array}\right. \qquad \cdots\cdots\cdots\cdots(\mathrm{A}\cdot 2)$$

The wave exciting forces and moments of longitudinal motions are given as follows.

$$\left[\begin{array}{l} F_{ze}=F_{zc}\cos\omega_e t-F_{zs}\sin\omega_e t \\ M_{\theta e}=M_{\theta c}\cos\omega_e t-M_{\theta s}\sin\omega_e t \end{array}\right. \quad \cdots\cdots\cdots\cdots (\mathrm{A}\cdot 3)$$

$$\begin{aligned}\begin{bmatrix}F_{zc}\\ F_{zs}\end{bmatrix}=&\begin{bmatrix}-\\ +\end{bmatrix}2\rho g\zeta_a\int_L\begin{bmatrix}\cos\\ \sin\end{bmatrix}(m_0x_b\cos\mu)\int_0^b\frac{\cosh m_0(h-z_s)}{\cosh m_0h}\cos(m_0y_s\sin\mu)dy_sdx_b\\ &\begin{bmatrix}+\\ -\end{bmatrix}\zeta_a\int_L\frac{\sinh m_0(h-T_m)}{\sinh m_0h}\cdot\omega\omega_eM_H\begin{bmatrix}\cos\\ \sin\end{bmatrix}(m_0x_b\cos\mu)dx_b\\ &-\zeta_a\int_L\frac{\sinh m_0(h-T_m)}{\sinh m_0h}\cdot\omega N_H\begin{bmatrix}\sin\\ \cos\end{bmatrix}(m_0x_b\cos\mu)dx_b.\end{aligned} \quad \cdots\cdots\cdots\cdots (\mathrm{A}\cdot 4)$$

$$\begin{aligned}\begin{bmatrix}M_{\theta c}\\ M_{\theta s}\end{bmatrix}=&\begin{bmatrix}-\\ +\end{bmatrix}2\rho g\zeta_a\int_Lx_b\begin{bmatrix}\cos\\ \sin\end{bmatrix}(m_0x_b\cos\mu)\int_0^b\frac{\cosh m_0(h-z_s)}{\cosh m_0h}\cos(m_0y_s\sin\mu)dy_sdx_b\\ &\begin{bmatrix}+\\ -\end{bmatrix}\zeta_a\int_L\frac{\sinh m_0(h-T_m)}{\sinh m_0h}\left(\omega\omega_eM_Hx_b-\frac{\omega}{\omega_e}VN_H\right)\begin{bmatrix}\cos\\ \sin\end{bmatrix}(m_0x_b\cos\mu)dx_b\\ &-\zeta_a\int_L\frac{\sinh m_0(h-T_m)}{\sinh m_0h}(\omega N_Hx_b+\omega VM_H)\begin{bmatrix}\sin\\ \cos\end{bmatrix}(m_0x_b\cos\mu)dx_b.\end{aligned} \quad (\mathrm{A}\cdot 5)$$

The coefficients for lateral motions:

$$\left[\begin{array}{ll} A_{22}=\int_L M_Sdx_b, & B_{22}=\int_L N_Sdx_b, \\ A_{26}=\int_L M_Sx_bdx_b+\frac{V}{\omega_e^2}\int_L N_Sdx_b, & B_{26}=\int_L N_Sx_bdx_b-V\int_L M_Sdx_b, \\ A_{24}=\int_L M_S(\overline{OG}-l_{SR})dx_b, & B_{24}=\int_L N_S(\overline{OG}-l_w)dx_b. \end{array}\right. \quad \cdots\cdots\cdots (\mathrm{A}\cdot 6)$$

$$\left[\begin{array}{l} A_{66}=\int_L M_Sx_b^2dx_b+\frac{V^2}{\omega_e^2}\int_L M_Sdx_b, \quad B_{66}=\int_L N_Sx_b^2dx_b+\frac{V^2}{\omega_e^2}\int_L N_Sdx_b, \\ A_{64}=\int_L M_S(\overline{OG}-l_{SR})\,x_bdx_b-\frac{V}{\omega_e^2}\int_L N_S(\overline{OG}-l_w)dx_b, \\ B_{64}=\int_L N_S\,(\overline{OG}-l_w)\,x_bdx_b+V\int_L M_S(\overline{OG}-l_{SR})dx_b, \\ A_{62}=\int_L M_Sx_bdx_b-\frac{V}{\omega_e^2}\int_L N_Sdx_b, \qquad B_{62}=\int_L N_Sx_bdx_b+V\int_L M_Sdx_b. \end{array}\right. \quad \cdots (\mathrm{A}\cdot 7)$$

$$\left\{\begin{array}{l} A_{44}=\int_L M_S(l_{SR}l_{RS}-2\overline{OG}\cdot l_{SR}+\overline{OG}^2)dx_b, \\ B_{44}=\int_L N_S(\overline{OG}-l_w)^2 dx_b, \qquad C_{44}=W\cdot\overline{GM}, \\ A_{42}=\int_L M_S(\overline{OG}-l_{SR})dx_b, \qquad B_{42}=\int_L N_S(\overline{OG}-l_w)dx_b, \\ A_{46}=\int_L M_S(\overline{OG}-l_{SR})x_b dx_b+\dfrac{V}{\omega_e^2}\int_L N_S(\overline{OG}-l_w)dx_b, \\ B_{46}=\int_L N_S(\overline{OG}-l_w)x_b dx_b-V\int_L M_S(\overline{OG}-l_{SR})dx_b. \end{array}\right. \quad \cdots\cdots\cdots (A\cdot 8)$$

The wave exciting forces and moments of lateral motions are given as follows.

$$\left\{\begin{array}{l} F_{ye}=F_{yc}\cos\omega_e t-F_{ys}\sin\omega_e t \\ M_{\phi e}=M_{\phi c}\cos\omega_e t-M_{\phi s}\sin\omega_e t \\ M_{\psi e}=M_{\psi c}\cos\omega_e t-M_{\psi s}\sin\omega_e t \end{array}\right. \quad \cdots\cdots\cdots\cdots (A\cdot 9)$$

$$\begin{aligned} \begin{bmatrix} F_{yc} \\ F_{ys} \end{bmatrix} &= -2\rho g\zeta_a\int_L \begin{bmatrix} \sin \\ \cos \end{bmatrix}(m_0 x_b\cos\mu)\int_0^T \frac{\cosh m_0(h-z_s)}{\cosh m_0 h}\sin(m_0 y_s\sin\mu)dz_s dx_b \\ &-\zeta_a\sin\mu\int_L \omega\omega_e M_S\frac{\cosh m_0(h-T/2)}{\sinh m_0 h}\begin{bmatrix} \sin \\ \cos \end{bmatrix}(m_0 x_b\cos\mu)dx_b \\ &\begin{bmatrix} - \\ + \end{bmatrix}\zeta_a\sin\mu\int_L \omega N_S\frac{\cosh m_0(h-T/2)}{\sinh m_0 h}\begin{bmatrix} \cos \\ \sin \end{bmatrix}(m_0 x_b\cos\mu)dx_b. \end{aligned} \quad \cdots\cdots (A\cdot 10)$$

$$\begin{aligned} \begin{bmatrix} M_{\phi c} \\ M_{\phi s} \end{bmatrix} &= \overline{OG}\cdot\begin{bmatrix} F_{yc} \\ F_{ys} \end{bmatrix}-2\rho g\zeta_a\int_L \begin{bmatrix} \sin \\ \cos \end{bmatrix}(m_0 x_b\cos\mu)\left\{\int_0^b \frac{\cosh m_0(h-z_s)}{\cosh m_0 h}y_s\sin(m_0 y_s\sin\mu)dy_s\right. \\ &\left.-\int_0^T \frac{\cosh m_0(h-z_s)}{\cosh m_0 h}z_s\sin(m_0 y_s\sin\mu)dz_s\right\}dx_b \\ &+\zeta_a\sin\mu\int_L \omega\omega_e M_S l_{SR}\frac{\cosh m_0(h-T/2)}{\sinh m_0 h}\begin{bmatrix} \sin \\ \cos \end{bmatrix}(m_a x_b\cos\mu)dx_b \\ &\begin{bmatrix} + \\ - \end{bmatrix}\zeta_a\sin\mu\int_L \omega N_S l_w\frac{\cosh m_0(h-T/2)}{\sinh m_0 h}\begin{bmatrix} \cos \\ \sin \end{bmatrix}(m_0 x_b\cos\mu)dx_b. \end{aligned} \quad \cdots\cdots\cdots\cdots (A\cdot 11)$$

$$\begin{aligned} \begin{bmatrix} M_{\psi c} \\ M_{\psi s} \end{bmatrix} &= -2\rho g\zeta_a\int_L x_b\begin{bmatrix} \sin \\ \cos \end{bmatrix}(m_0 x_b\cos\mu)\int_0^T \frac{\cosh m_0(h-z_s)}{\cosh m_0 h}\sin(m_0 y_s\sin\mu)dz_s dx_b \\ &-\zeta_a\sin\mu\int_L \frac{\cosh m_0(h-T/2)}{\sinh m_0 h}\left(\omega\omega_e M_S x_b-\frac{\omega}{\omega_e}VN_S\right)\begin{bmatrix} \sin \\ \cos \end{bmatrix}(m_0 x_b\cos\mu)dx_b \end{aligned}$$

$$\begin{bmatrix} - \\ + \end{bmatrix} \zeta_a \sin \mu \int_L \frac{\cosh m_0(h-T/2)}{\sinh m_0 h} (\omega N_S x_b + \omega V M_S) \begin{bmatrix} \cos \\ \sin \end{bmatrix} (m_0 x_b \cos \mu) dx_b. \qquad \cdots\cdots\cdots\cdots (A \cdot 12)$$

where the origine of coordinate system fixed in the ship body is coincident with the center of gravity of the ship, and

m_0 : wave number in water of finite depth
(a real root of equation: $\left(\frac{\omega^2}{g}\right) = m_0 \tan m_0 h$)
h : depth of water
ω_e : encounter circular frequency ($= \omega - m_0 V \cos \mu$)
ζ_a : amplitude of incident wave
ρ : density of water
g : gravitational acceleration
T_m : mean draft (S_x / B_x)
M_H, M_S : sectional added mass for heave and sway
N_H, N_S : sectional damping force for heave and sway
l_{SR} : lever of sectional added moment of inertia due to sway
l_w : lever of sectional damping moment due to sway